Int. J. Heat Mass Transfer. Vol. 13, pp. 753–787. Pergamon Press 1970. Printed in Great Britain

EXPERIMENTS ON NATURAL-CONVECTION HEAT TRANSFER FROM THE OUTER SURFACE OF A VERTICAL CYLINDER TO LIQUIDS

T. FUJII, M. TAKEUCHI, M. FUJII, K. SUZAKI and H. UEHARA
Research Institute of Industrial Science, Kyushu University, Fukuoka, Japan

(*Received* 16 *December* 1968)

Abstract—This paper describes the results of experimental investigations on natural-convection heat transfer from the outer surface of a vertical cylinder one metre high to water, spindle oil and Mobiltherm oil. The characteristics of the experiments are as follows. The experimental apparatus is contrived to enable us to measure local heat transfer coefficients directly; sufficiently long turbulent boundary layers are made to appear under various conditions of temperature and heat flux of the heated cylinder; correspondences of local heat transfer coefficients with flow patterns are clarified from the observations of the boundary layer by means of "mirage method" or other methods, and from the measurements of temperature profiles in it; the influence of Prandtl number upon heat transfer is found in its range from 2 to 2600.

The boundary layer develops through laminar, vortex-street, transition-turbulent and turbulent flow pattern, and each flow pattern has respective characteristics of heat transfer. Vortex-street flow provokes abrupt increase of heat transfer coefficients in the transitional region from laminar to transition-turbulent. Especially with respect to water, no distinction was found between transition-turbulent and turbulent flow, and its cause is explained by an indeterminate character of the flow pattern in the transitional region.

Local heat transfer coefficients are correlated nondimensionally about each flow region in the cases of uniform wall temperature and uniform heat flux. In each case, two kinds of experimental equations are proposed, respectively, by using the physical properties at a reference temperature and by using the supplementary terms referred to the variation of kinematic viscosity. Non-dimensional equations of average heat transfer coefficients are also proposed for the case of uniform wall temperature. Furthermore, some remarks on the ranges applicable to each equation are presented.

The shapes of vortex-pairs, laminar sub-layers and turbulent lumps in the boundary layer as well as their development, are clearly taken in "mirage" photos. The transitions of flow patterns are also concretely described.

Temperature fluctuations in the boundary layer are revealed and the time-mean temperature profiles are represented by a non-dimensional parameter.

"Quasi-steady state" is defined experimentally as a state equivalent to a steady state with respect to heat transfer coefficients.

NOMENCLATURE

c, specific heat at constant pressure [J/Kg grd];

D, diameter of the heated cylinder [m];

Gr_L, average Grashof number $= \dfrac{L^3 g\beta(t_0 - t_\infty)}{\nu^2}$;

Gr_x, local Grashof number $= \dfrac{x^3 g\beta(t_0 - t_\infty)}{\nu^2}$;

Gr_x^* modified local Grashof number $= \dfrac{x^4 g\beta q}{\nu^2\lambda} = Nu_x Gr_x$;

g, gravitational acceleration [m/s^2];

L, height of the heated cylinder [m];

Nu_L, average Nusselt number $= \dfrac{\alpha_L L}{\lambda}$;

Nu_x, local Nusselt number $= \dfrac{\alpha_x x}{\lambda}$;

Pr, Prandtl number $= \frac{\nu}{\kappa}$;
Q, heat transfer rate per unit section of the heated cylinder [W];
q, heat flux at the wall of the heated cylinder [W/m^2];
t, temperature [°C];
x, distance vertically upward from the lower end of the heated cylinder [m];
y, distance normally away from the heated cylinder [m].

Greek symbols

α_L, average heat transfer coefficient [W/m^2 grd];
α_x, local heat transfer coefficient [W/m^2 grd];
β, average volumetric thermal expansion coefficient $= \frac{\rho_\infty - \rho_m}{\rho_m(t_m - t_\infty)}$ [1/grd];
ρ, density [Kg/m^3];
δ, thickness of the temperature boundary layer defined in equation (28) [m];
ζ, correlation variable i.e. non-dimensional distance in y direction defined in equation (29);
θ, non-dimensional temperature $= \frac{(t - t_\infty)}{(t_0 - t_\infty)}$;
κ, thermal diffusivity $= \frac{\lambda}{c\rho}$ [m^2/s];
λ, thermal conductivity [W/m grd];
ν, kinematic viscosity [m^2/s].

Subscripts

cri, conditions at the upper limit of laminar region;
i, i'th section of the cylinder from the lowest, and conditions at its middle height;
j, conditions at the upper end of the i'th section;
l, conditions on the level of the lowest end of the heated cylinder;
m, conditions at the film temperature defined in equation (6);
0, conditions on the wall of the heated cylinder;
∞, conditions in the ambient fluid;
x, local value at x;
$( )_e$, physical properties at the temperature t_e defined in equation (7) are employed;
$( )_\infty$, physical properties at the temperature t_∞ are employed.

1. INTRODUCTION

THROUGH previous experiments on natural convection in ethylene-glycol along a relatively short vertical cylinder, Fujii [1–3], one of the authors, demonstrated that local Nu number is proportional to the one-fourth power of Gr number, not only in laminar region but also in turbulent one. He inferred theoretically that it would successively undergo transition to the region in which local Nu number is proportional to the two-fifths power of Gr number, and named the former region transition-turbulent and the latter turbulent respectively. Recently, Cheesewright [4] measured local heat transfer coefficients of natural convection in air along a vertical flat plate. In his data on turbulent heat transfer we can also recognize the distinction between those two regions. On the other hand, it is commonly recommended that local Nu number is proportional to the one-third power of Gr number with respect to turbulent heat transfer [5]. Not only in trend but also in magnitude, non-dimensional equations of heat transfer coefficients in turbulent region are uncertain.

As for the approximate theory to evaluate turbulent heat transfer coefficients, no quantitatively reliable values have been obtained, since the solutions of Fujii [3] and Eckert and Jackson [6] are based on inaccurate assumptions especially for the velocity and temperature profiles in the boundary layer. On the other hand, Kato *et al.* [7] solved the fundamental differential equations of natural convection by assuming the eddy diffusivity based on analogical inference from forced convection. Their solutions are, however, different qualitatively from the above-

mentioned approximate ones and the range of their application has not been proved experimentally.

On the mechanism of the transition from laminar to turbulent flow, Eckert and Soehngen [8] found the waves which resembled the Tollmien–Schlichting waves, and Szewczyk [9] observed the waves to be amplified and transformed further into double-row vortex system. The cause of the transition is usually explained by the analogical inference from forced convection. Szewczyk's stability calculations based on the small perturbation theory, however, did not agree with his experimental results. Fujii [10] proposed a different interpretation to the similar observation, but it was not strictly correct. Furthermore, no clear-cut relation between the transition processes of flow patterns and the local variation of heat transfer coefficients was given in Fujii's statement as well as in Szewczyk's.

When performing experiments to make clear the uncertain problems above-mentioned, we have to consider several matters as follows. Local heat transfer coefficients should be directly measured over the range of the product $GrPr$ at least up to 10^{12} [2]; in the case of natural convection along a flat plate, no accurate two-dimensionality could be attained neither thermally nor fluid dynamically owing to the side effect; experimental results should be compared on various fluids of remarkably different Pr number; especially, high viscous fluid should be used, because the higher is viscosity of fluid, the longer persist the vortices in the boundary layer. The authors therefore adopted a vertical cylinder of one meter height for the apparatus, and water, spindle oil and Mobiltherm oil for fluid.

Experimental results only are described in this paper. Accurate measurements on variations of local heat transfer coefficients over the range from laminar to fully developed turbulent flow are presented to induce non-dimensional experimental equations. The correspondences of the flow patterns, their transitions and the temperature profiles in the boundary layer, to the local heat transfer coefficients are clarified.

2. APPARATUS, INSTRUMENTATION AND RANGE OF EXPERIMENTS

The arrangement of the experimental apparatus is shown in Fig. 1. A vertical hollow brass cylinder of 82·0 mm o.d., 66·0 mm i.d. and 1000 mm height was made by soldering 20 cylinders of 50 mm height by pasty solder after piling on each other, by facing its outer surface with a lathe, and by lapping up the surface by emery paper and compound. In each unit

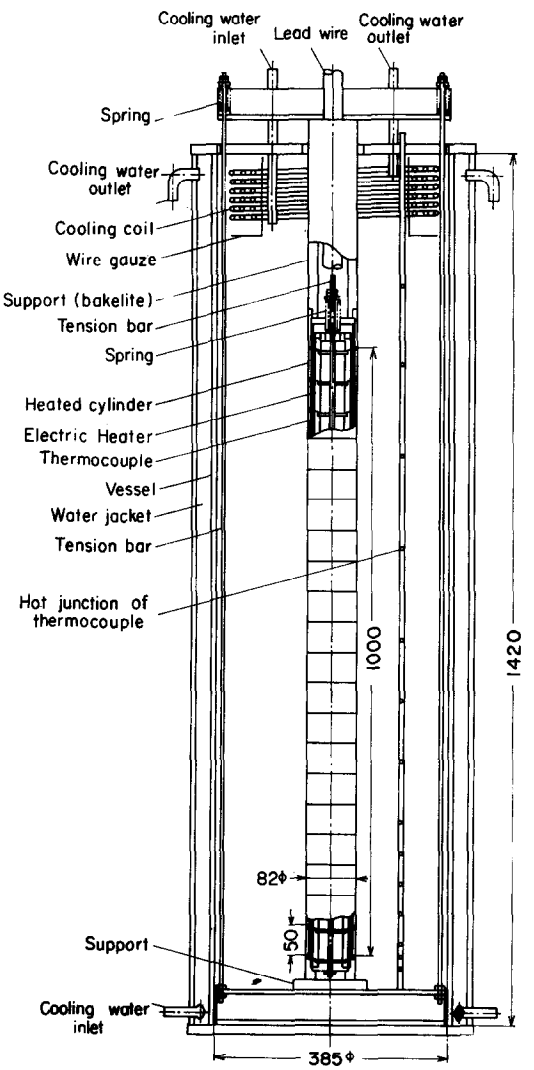

FIG. 1. Experimental apparatus.

cylinder, 10 longitudinal holes of 2 mm dia. had been drilled at circumferentially equal intervals and at the position of 3 mm from the inner surface. Each hole was overlapped so as to constitute one hole from the upper end to the lower end, in order to make it serve as the hole for inserting thermocouples. Each cylinder was soldered up to 3 mm depth from the outer surface of the cylinder. Whereas the non-soldered sections constituted a gap of 0·1 mm height up to the depth of 5 mm from the inner surface. The cylinder was heated indirectly by an electric heater, which was subdivided into 20 sections. The heater was constructed by piling up 20 bobbins made of fire-proof cement of 63 mm o.d. and 50 mm height, around which was wound 0·8 mm nichrome wire 30 times at 1·5 mm pitch. The details of one unit section of the cylinder and heater are shown in Fig. 2. Since the gap between the nichrome wire and the heated cylinder was 1·2 mm, 10 distance rings were set at the vertical interval of 100 mm to prevent electric short-circuit.

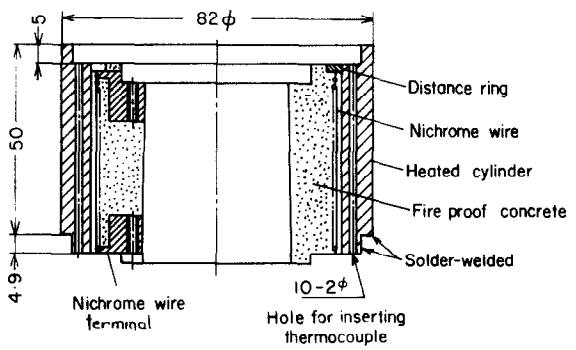

FIG. 2. Unit section of the heated cylinder and heater.

A cylindrical vessel of 385 mm i.d. and 1420 mm height was made of transparent acrylic acid resin to facilitate visual observation. In order to prevent the rise of ambient fluid temperature and to reduce the gradient of temperature stratification as much as possible, cooled water was circulated through the jacket of the vessel and a coil bank of copper pipes near the free surface of liquid. The coil bank was covered by wire gauze for diminishing turbulence.

For each condition of the experiments, it took several hours for the whole temperature of the apparatus to reach a steady state, and over ten hours for various kinds of measurement to be performed. In order to maintain the state steady during the run, the electric source of the heaters was kept at 100·0 $\pm$ 0·1 V by a constant-voltage regulator, and the temperature of the cooling water was appropriately controlled by a refrigerator and a 2 KW electric heater inserted in the cooling water circuit.

The electric current through each unit heater was regulated properly by each individual variable-voltage transformer. Since the power factor of each circuit was more than 0·999, the power was measured by a iron-vain type voltmeter and ammeter of 0·5 per cent accuracy. The electric inputs to the heaters of the lowest one and uppermost two sections were oversupplied by the amount of conductive heat losses through the supporting assembly of the heated cylinder and the electric lead wires. The measured values corresponding to these sections, therefore, were not taken up in the correlated data.

Two copper–constantan thermocouples of 0·30 mm dia. were inserted into each 2 mm hole of the heated cylinder from its upper end. The hot junctions of them were electrically insulated and placed respectively as high as the center of each subdivided unit section of the heated cylinder. Each remaining hollow in the hole from the lower end up to the hot junction was stuffed with copper wire. The temperature on the outer surface of the heated cylinder, namely wall temperature, was obtained by correcting the indication of each thermocouple in proportion to the heat flux at the point. For the measurement of ambient fluid temperature, 14 copper–constantan thermocouples of 0·32 mm dia. were placed at the middle distance between the heated cylinder and the vessel. The position of each hot junction is shown in Fig. 1 and each thermocouple was bent for a distance of 50 mm

from its hot junction horizontally and circumferentially. The electro-motive forces of the thermocouples were mostly printed on the strip-charts of two sets of self-balancing electronic recorders (24 points self-switching, 5 and 10 mV full-scale, 5 μV sensitivity).

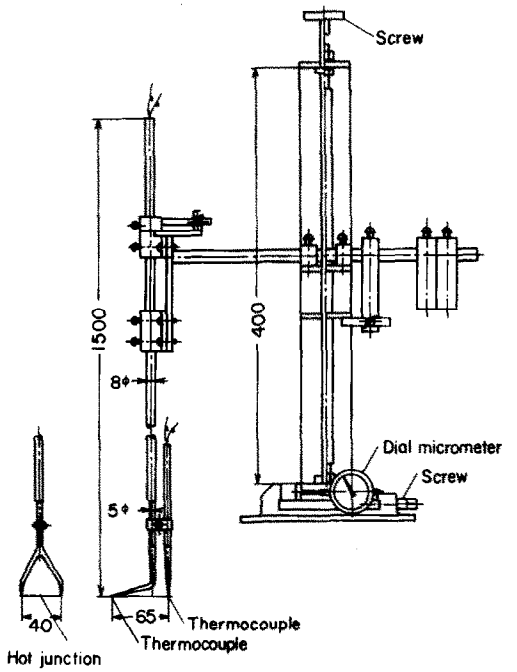

FIG. 3. Thermocouple probe and its traversing assembly.

The temperature field in the boundary layer was measured by a thermocouple probe shown in Fig. 3. The probe body was fabricated from glass tubes in the shape of a two-tined fork, and the distance between the tines was 40 mm. The thermocouple, fabricated from 0·05 mm copper and constantan wire, was suspended between the tips of the tines. The junction was formed at the center of the 40 mm span by butt-welding the two materials. The traversing assembly was constructed by utilizing screws of vices, and the horizontal travel was measured by a mechanical dial micro-meter capable of detecting lengths to within 0·01 mm in 10 mm. The coordinate of the hot junction from the wall of the heated cylinder was determined by linearly exterpolating the measurements close to the wall up to the temperature measured by the thermocouple inserted in the heated cylinder. The discrepancy between the coordinate thus determined and that determined preliminarily by telescopic observation was of the order from 0·05 to 0·4 mm. The vertical distance of the hot junction from the lower end of the heated cylinder was adjusted manually prior to each traverse, and read by a cathometer capable of detecting heights to within 0·05 mm in 1000 mm.

In order to measure the temperature fluctuations in the boundary layer and of the heated cylinder, the direct current component of the thermo-electro-motive force was cancelled by adding appropriate negative electric voltage by means of a potentiometer, then the fluctuating component was amplified by pen recorder. These records include more or less time lag and amplitude damping.

Deaerated pure water of about 2 MΩcm specific resistance, white spindle oil and Mobiltherm 600 oil were employed for fluid. The physical properties of water were based on [11], and those of oils were measured prior to use in our laboratory. The variation of each value with temperature was expressed by an approximate formula as shown in the Appendix.

The ranges of experiments are shown in Table 1. Nondimensional values of the data were calcaulted by an electronic computer OKITAC 5090H in the Computation Center of Kyushu University.

3. "MIRAGE METHOD" FOR OBSERVATION OF THE BOUNDARY LAYER

The boundary layer flow was observed by means of dye injection, shadow graph and "mirage method", which was originated in this investigation. The photographic records by mirage method are mainly adopted in this paper for illustration.

Black wires of 2·2 mm dia. and about 1·3 m length were arranged in stripes at 4·5 mm pitch

Table 1. Ranges of experiments

Fluid	Water		White spindle oil		Mobiltherm 600 oil	
Experimental condition	t_0 uniform	q uniform	t_0 uniform	q uniform	t_0 uniform	q uniform
Surface temperature t_0(°C)	26–71	21–86	56–147	62–180	75–152	70–157
Fluid temperature t_∞(°C)	16–44	14–43	22–59	28–55	21–62	22–57
Heat flux q (W/m^2)	$2{\cdot}1 \times 10^3$–$2{\cdot}7 \times 10^4$	$2{\cdot}4 \times 10^3$–$3{\cdot}0 \times 10^4$	$1{\cdot}9 \times 10^3$–$1{\cdot}9 \times 10^4$	$3{\cdot}8 \times 10^3$–$3{\cdot}1 \times 10^4$	$2{\cdot}2 \times 10^3$–$1{\cdot}4 \times 10^4$	$3{\cdot}9 \times 10^3$–$1{\cdot}2 \times 10^4$
Prandtl number $(Pr)_e$	2·8–6·4	2·4–7·1	24–92	19–79	41–240	42–300
$(Pr)_\infty$	4·0–7·9	4·1–8·2	77–170	76–170	260–2600	310–2600
Grashof number $(Gr_x)_e$, $(Gr_x^*)_e$	$7{\cdot}2 \times 10^6$–$4{\cdot}3 \times 10^{11}$	$1{\cdot}5 \times 10^8$–$5{\cdot}8 \times 10^{14}$	$2{\cdot}5 \times 10^6$–$2{\cdot}2 \times 10^{11}$	$2{\cdot}5 \times 10^8$–$9{\cdot}6 \times 10^{14}$	$4{\cdot}0 \times 10^5$–$5{\cdot}8 \times 10^{10}$	$1{\cdot}3 \times 10^7$–$5{\cdot}0 \times 10^{13}$
$(Gr_x)_\infty$, $(Gr_x^*)_\infty$	$5{\cdot}0 \times 10^6$–$2{\cdot}2 \times 10^{11}$	$1{\cdot}2 \times 10^8$–$3{\cdot}1 \times 10^{14}$	$4{\cdot}8 \times 10^5$–$2{\cdot}3 \times 10^{10}$	$5{\cdot}4 \times 10^7$–$8{\cdot}3 \times 10^{13}$	$3{\cdot}4 \times 10^3$–$1{\cdot}3 \times 10^9$	$1{\cdot}7 \times 10^5$–$9{\cdot}4 \times 10^{11}$
$(Gr_xPr)_e$, $(Gr_x^*Pr)_e$	$4{\cdot}6 \times 10^7$–$1{\cdot}2 \times 10^{12}$	$1{\cdot}1 \times 10^9$–$1{\cdot}6 \times 10^{15}$	$2{\cdot}2 \times 10^8$–$5{\cdot}3 \times 10^{12}$	$2{\cdot}0 \times 10^{10}$–$1{\cdot}9 \times 10^{16}$	$9{\cdot}6 \times 10^7$–$2{\cdot}4 \times 10^{12}$	$4{\cdot}0 \times 10^9$–$2{\cdot}4 \times 10^{15}$
$(Gr_xPr)_\infty$, $(Gr_x^*Pr)_\infty$	$4{\cdot}0 \times 10^7$–$8{\cdot}9 \times 10^{11}$	$9{\cdot}6 \times 10^8$–$1{\cdot}3 \times 10^{15}$	$9{\cdot}6 \times 10^7$–$1{\cdot}6 \times 10^{12}$	$8{\cdot}8 \times 10^9$–$4{\cdot}1 \times 10^{15}$	$8{\cdot}9 \times 10^6$–$3{\cdot}5 \times 10^{11}$	$4{\cdot}2 \times 10^8$–$3{\cdot}0 \times 10^{14}$
Nusselt number $(Nu_x)_e$	40–1440	41–1370	60–1850	72–2250	59–1100	51–1110
$(Nu_x)_\infty (v_0/v_\infty)^{0{\cdot}21}$, $(Nu_x)_\infty (v_0/v_\infty)^{0{\cdot}17}$	39–1210	38–1300	57–1290	61–1630	28–700	32–740

Values of Gr_x, Gr_xPr and $Nu_x(v_0/v_\infty)^{0{\cdot}21}$ are entered in respective columns of uniform wall temperature and Gr_x^*, Gr_x^*Pr and $Nu_x(v_0/v_\infty)^{0{\cdot}17}$ in respective columns of uniform heat flux.

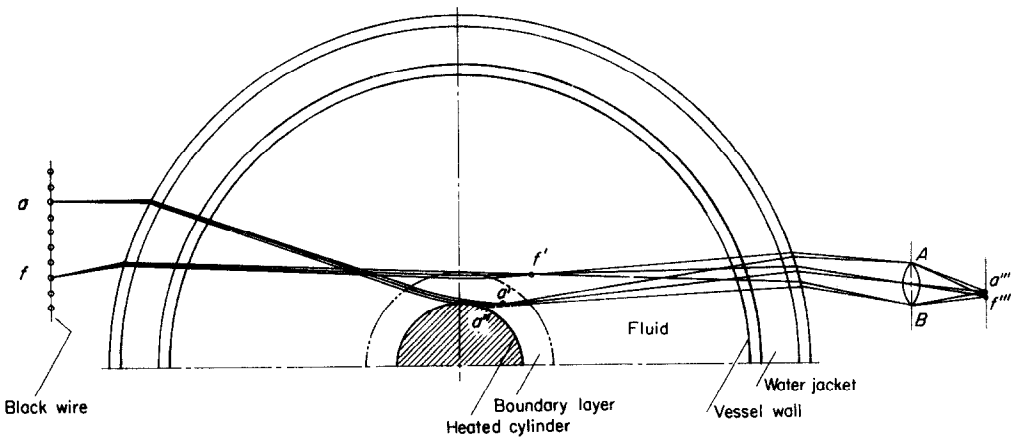

FIG. 4. Principle of "mirage method".

on a milk-white plate made of acrylic acid resin. The setting was stood against the vessel, and lightened uniformly from the backside of the plate. When we observe the vicinity of the heated cylinder from the opposite side of the vessel, we can find the refracted images of the wire stripes corresponding to the temperature field in the boundary layer.

The principle of this phenomenon is shown in Fig. 4. The light beam is bent more when it passes through nearer to the heated cylinder, because the refractive index of the fluid in the boundary layer decreases with temperature rise. When the wire stripes and a camera or a naked eye are set as shown in the figure respectively, for example, image a′ of wire a is focussed owing to the refraction in the boundary layer and furthermore image a‴ on the film or the retina by its lens. Since such a light beam as a–a‴, which focusses once at a′ in the boundary layer, is bent further by the temperature field, image a‴ on the film corresponds to ghost image a″. The light beams that enter the lens of bore AB through the boundary layer are limited to the range between a–a‴ and f–f‴. Since the light beams corresponding to each image are restricted within an extremely narrow zone in the boundary layer, we can reveal the local feature of the temperature field. The authors name this method of observation "mirage method" from analogy to a mirage phenomenon. In the case of water the mirage image is rather ambiguous compared with the case of spindle oil. Besides, this mirage method seems to be inappropriate for the observation of the boundary layer in air, refractive index of which varies scarcely with temperature.

For taking photos, a Nikon motor-drive camera and a Bolex movie camera were used.

4. EXPERIMENTAL RESULTS AND CONSIDERATION

4.1 *Non-dimensional expressions of local heat transfer coefficients by the physical properties at a reference temperature*

Representative distributions of ambient fluid temperature t_∞, wall temperature t_0 and heat flux q in the cases of uniform wall temperature and uniform heat flux are shown respectively in Figs. 5(a), (b) for water and Figs. 6(a), (b) for spindle oil. The horizontal bars drawn on the curves of the wall temperature in Fig. 5 indicate the maximum amplitudes obtained from the records of its fluctuations. For the time being, we take up only the time-mean values for

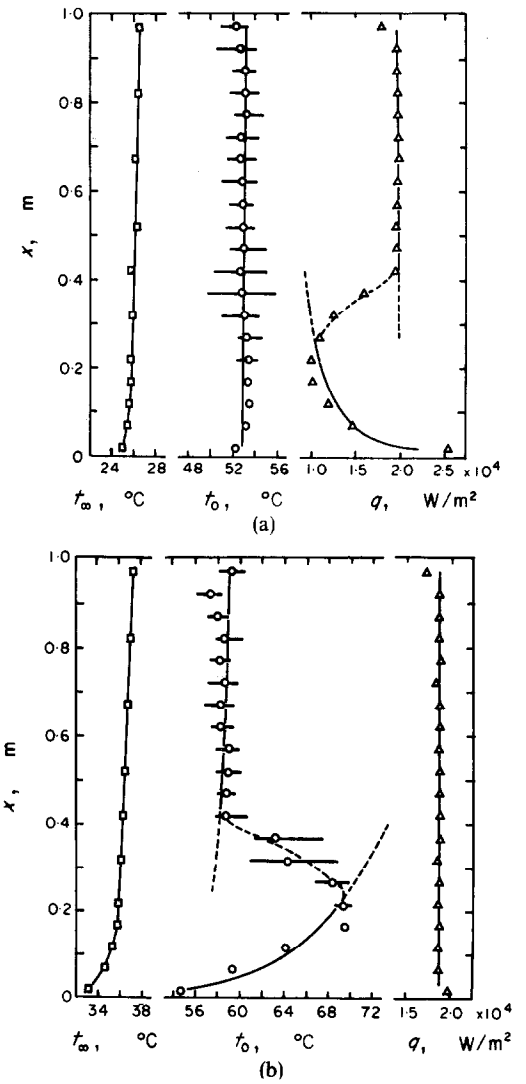

FIG. 5. Distributions of ambient fluid temperature t_∞, wall temperature t_0 and heat flux q for water.
(a) uniform wall temperature. (b) uniform heat flux.

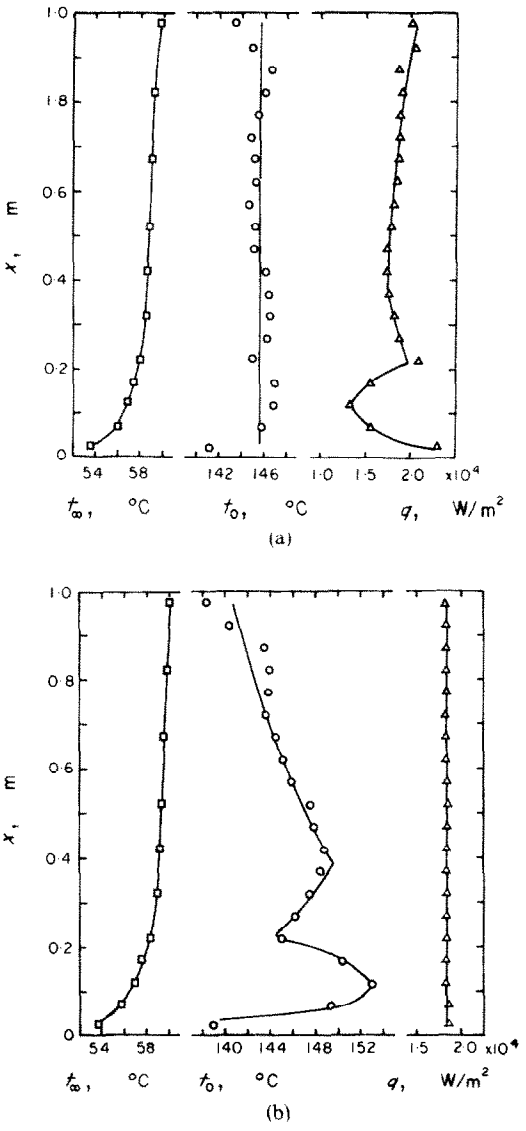

FIG. 6. Distributions of ambient fluid temperature t_∞, wall temperature t_0 and heat flux q for spindle oil.

(a) uniform wall temperature. (b) uniform heat flux.

consideration, leaving the fluctuation itself and its influence on heat transfer for reconsideration in section 4.6.

Local heat transfer coefficient α_x, local Nu number Nu_x, local Gr number Gr_x, and local modified Gr number Gr_x^* in the case of uniform heat flux are evaluated by the following equations respectively;

$$\alpha_x = \frac{Q_i}{\pi D(x_j - x_j^{-1})(t_0 - t_\infty)_i} = \frac{q_i}{(t_0 - t_\infty)_i}, \quad (1)$$

$$Nu_x = \frac{\alpha_x x_i}{\lambda}, \quad (2)$$

$$Gr_x = \frac{x_i^3 g\beta(t_0 - t_\infty)_i}{\nu^2}, \quad (3)$$

$$Gr_x^* = \frac{x_i^4 g\beta q_i}{\nu^2 \lambda}, \quad (4)$$

where

$$x_i = \frac{x_j + x_{j-1}}{2}, (i,j = 1,2,\ldots.20), \quad (5)$$

and subscript i signifies the i'th subdivided section of the heated cylinder from the lowest and subscript j conditions at its upper end.

In this section are attempted non-dimensional expressions of local heat transfer coefficients by means of the physical properties corresponding to a reference temperature, which represents the temperature distributed in the boundary layer. Figure 7 shows a preliminary plot of Nu_x vs. Gr_xPr with respect to two different temperature conditions of the heated cylinder in spindle oil. Four kinds of temperature t_∞, t_m, t_e and t_0 are taken as a reference temperature, where

$$t_m = \tfrac{1}{2}(t_0 + t_\infty), \quad (6)$$

and

$$t_e = t_0 - \tfrac{1}{4}(t_0 + t_\infty). \quad (7)$$

In each case, however, β is evaluated on the basis of t_∞ and t_m. The data corresponding to t_e are in good correlation as a whole, and furthermore, the data of the group of lower Gr_xPr are in good agreement with the numerical solution based on the laminar boundary layer theory [12]. The same holds also for the data on water. Accord-

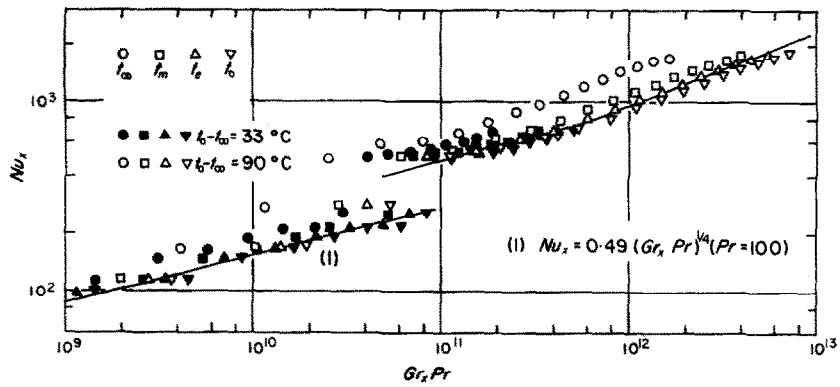

FIG. 7. Preliminary plot of Nu_x vs. Gr_xPr for spindle oil by using the physical properties at t_∞, t_m, t_e and t_0 respectively.

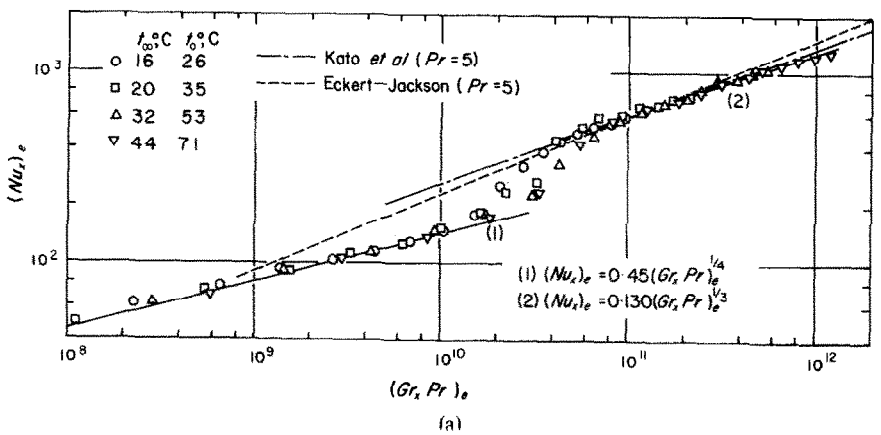

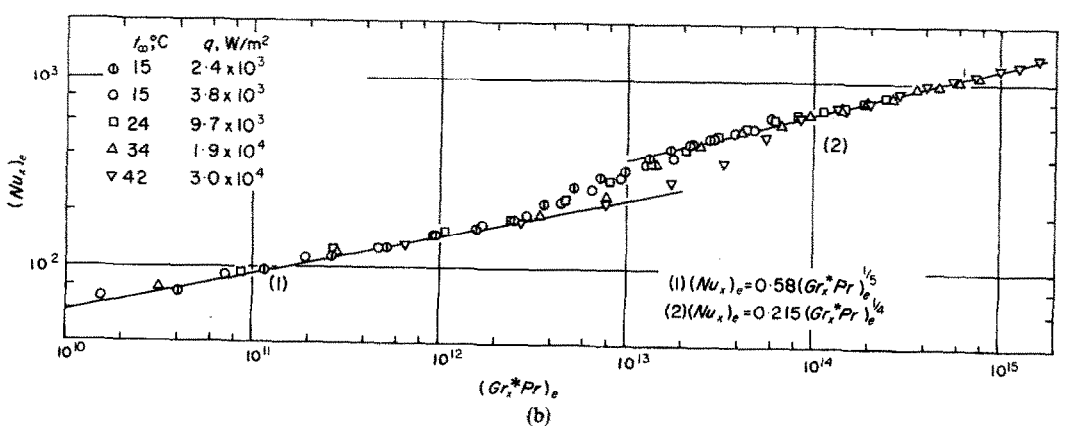

FIG. 8. Non-dimensional correlation of α_x for water. (a) uniform wall temperature. (b) uniform heat flux.

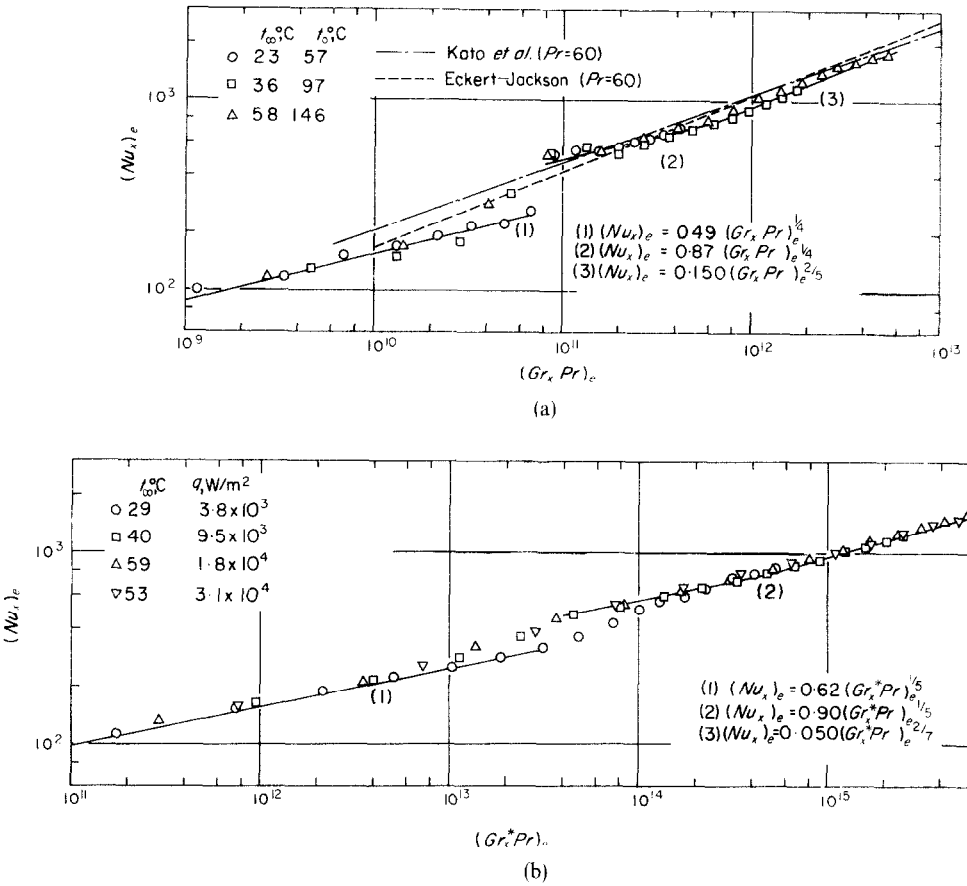

FIG. 9. Non-dimensional correlation of α_x for spindle oil. (a) uniform wall temperature. (b) uniform heat flux.

ingly, the non-dimensional numbers in this section are evaluated at the reference temperature t_e and these are signified by $(\ )_e$. By the way, thus determined reference temperature t_e agrees with that induced from Fujii's approximate solutions on the laminar boundary layer equations of ethylene-glycol [13] as well as from Akagi's numerical solutions on the laminar boundary layer equations of high viscous mineral oils [14].

Figures 8(a),(b), 9(a),(b) and 10(a),(b) show the data on water, spindle oil and Mobiltherm oil respectively, where the plots of $(Nu_x)_e$ vs. $(Gr_x Pr)_e$ and $(Nu_x)_e$ vs. $(Gr_x^* Pr)_e$ correspond to the cases of uniform wall temperature and uniform heat flux respectively. In each figure is drawn a line corresponding to the numerical solution of the laminar boundary layer equations on a vertical plate for $Pr = 5$ or 100 as an average [15,12]. That is, in the case of uniform wall temperature,

$$(Nu_x)_e = 0.45\,(Gr_x Pr)_e^{\frac{1}{4}}, (Pr = 5), \quad (8)$$

for water,

$$(Gr_x Pr)_e \leqslant (1 \sim 3) \times 10^{10};$$

$$(Nu_x)_e = 0.49\,(Gr_x Pr)_e^{\frac{1}{4}}, (Pr = 100), \quad (9)$$

for spindle oil,

$$(Gr_x Pr)_e \leqslant (3 \sim 7) \times 10^{10};$$

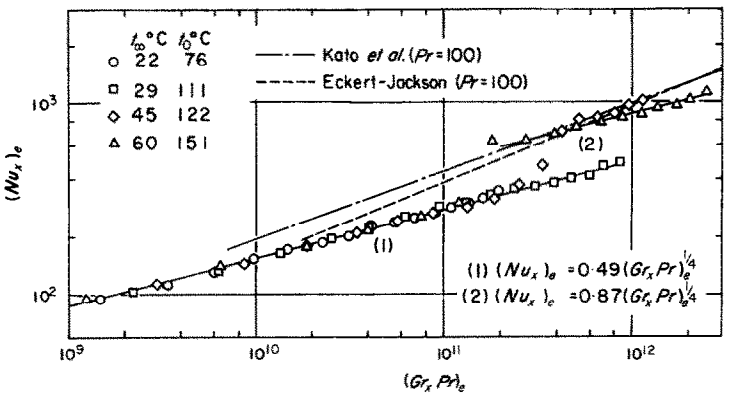

(a)

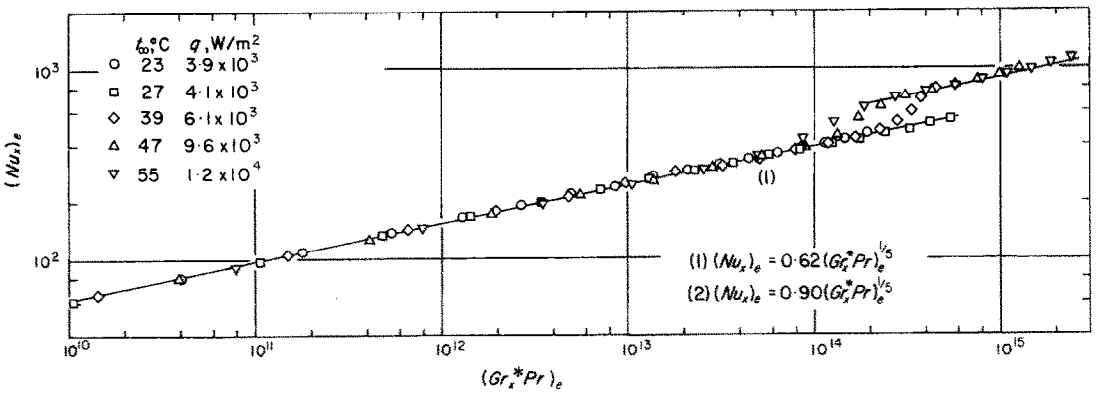

(b)

FIG. 10. Non-dimensional correlation of α_x for Mobiltherm oil. (a) uniform wall temperature. (b) uniform heat flux.

for Mobiltherm oil,

$$(Gr_x Pr)_e \leqslant (1{\cdot}5 \sim 9) \times 10^{11};$$

and in the case of uniform heat flux,

$$(Nu_x)_e = 0{\cdot}58\,(Gr_x^* Pr)_e^{\frac{1}{5}}, (Pr = 5), \quad (10)$$

for water,

$$(Gr_x^* Pr)_e \leqslant (0{\cdot}2 \sim 2) \times 10^{13};$$

$$(Nu_x)_e = 0{\cdot}62\,(Gr_x^* Pr)_e^{\frac{1}{5}}, (Pr = 100), \quad (11)$$

for spindle oil,

$$(Gr_x^* Pr)_e \leqslant (0{\cdot}5 \sim 3) \times 10^{13};$$

for Mobiltherm oil,

$$(Gr_x^* Pr)_e \leqslant (0{\cdot}6 \sim 6) \times 10^{14}.$$

Since the radius of the heated cylinder is sufficiently large compared with the boundary layer thickness, the heat transfer coefficients are estimated to be at most 1·3 per cent larger than those on a vertical heated plate [16], and these discrepancies are within the range of measurement accuracy. The experimental results are in good agreement with the theoretical ones in the range of $(Gr_x Pr)_e$ or $(Gr_x^* Pr)_e$ given to each equation.

For water, in the ranges of higher $(Gr_x Pr)_e$ and $(Gr_x^* Pr)_e$, the following equations are obtained

in the cases of uniform wall temperature and uniform heat flux respectively:

$$(Nu_x)_e = 0{\cdot}130\,(Gr_xPr)_e^{\frac{1}{3}}, (4 \sim 8) \times 10^{10} \leqslant (Gr_xPr)_e; \quad (12)$$

$$(Nu_x)_e = 0{\cdot}215\,(Gr_x^*Pr)_e^{\frac{1}{4}}, (1 \sim 7) \times 10^{13} \leqslant (Gr_x^*Pr)_e. \quad (13)$$

The ranges in which these equations hold, correspond to turbulent regions.

For spindle oil and Mobiltherm oil, successively arise the regions in which the non-dimensional experimental equations of heat transfer coefficients are represented as follows:

$$(Nu_x)_e = 0{\cdot}87\,(Gr_xPr)_e^{\frac{1}{3}}, \quad (14)$$

for spindle oil,
$8 \times 10^{10} \leqslant (Gr_xPr)_e \leqslant 6 \times 10^{11}$;

for Mobiltherm oil,
$(2 \sim 4) \times 10^{11} \leqslant (Gr_xPr)_e$;

$$(Nu_x)_e = 0{\cdot}90\,(Gr_x^*Pr)_e^{\frac{1}{4}}, \quad (15)$$

for spindle oil,
$(4 \sim 8) \times 10^{13} \leqslant (Gr_x^*Pr)_e \leqslant 5 \times 10^{14}$;

for Mobiltherm oil,
$(2 \sim 4) \times 10^{14} \leqslant (Gr_x^*Pr)_e$.

Fujii's experimental equation for ethylene-glycol [1] also shows an agreement with equation (14) in the range of $(Gr_xPr)_e$ from $8{\cdot}5 \times 10^9$ to 8×10^{10}. Furthermore in the experimental data on air of Cheesewright [4], such a region is also recognized as the heat transfer coefficients are represented by the same equation in the range of Gr_xPr from 6×10^9 to $2{\cdot}2 \times 10^{10}$.

For spindle oil, transitions take place further to the regions represented by the following equations:

$$(Nu_x)_e = 0{\cdot}0150\,(Gr_xPr)_e^{\frac{2}{3}}, \quad 6 \times 10^{11} \leqslant (Gr_xPr)_e; \quad (16)$$

$$(Nu_x)_e = 0{\cdot}050\,(Gr_x^*Pr_e^{\frac{1}{3}}, \quad 5 \times 10^{14} \leqslant (Gr_x^*Pr)_e. \quad (17)$$

For air also, according to Cheesewright's experiment [4], the similar transition takes place and the experimental equation may be expressed as:

$$(Nu_x) = 0{\cdot}0245\,(Gr_xPr)^{\frac{2}{3}}, \quad 2{\cdot}2 \times 10^{10} \leqslant (Gr_xPr). \quad (18)$$

For Mobiltherm oil, however, few data characteristic of this region were obtained, probably owing to the fact that sufficiently large values of $(Gr_xPr)_e$ or $(Gr_x^*Pr)_e$ were not attained.

The region in which the heat transfer coefficients are represented by equation (14) or (15) is named "transition-turbulent" region and that by the form of either equation (16), (17) or (18) "turbulent" region.

The characteristics about the non-dimensional expressions of heat transfer coefficients on a vertical wall may be summarized as follows.

(i) Non-dimensional correlations of heat transfer coefficients change in the order of laminar, transition-turbulent and turbulent region with the increase of $(Gr_xPr)_e$ or $(Gr_x^*Pr)_e$. For water, however, no distinction appeared between transition-turbulent and turbulent region. It seems to be an exceptional example, and the reason is stated in section 4.6.

(ii) Local Nu numbers are represented by the functions of the product Gr_xPr or Gr_2^*Pr over the whole regions from laminar to turbulent within the accuracy of the experiments.

(iii) Three pairs of equations (12), (13), (14), (15) and (16), (17) can be mutually transformed by the following equation:

$$Gr_x^* = Gr_xNu_x. \quad (19)$$

Namely, there is little difference, as far as the heat transfer in transition-turbulent and turbulent region is concerned, between the cases of uniform wall temperature and uniform heat flux. It does not hold, however, in laminar region, in which we cannot correctly induce equation (10) or (11) from equation (8) or (9) by the same transformation.

(iv) The fact that the data in transition-turbulent region are somewhat scattered es-

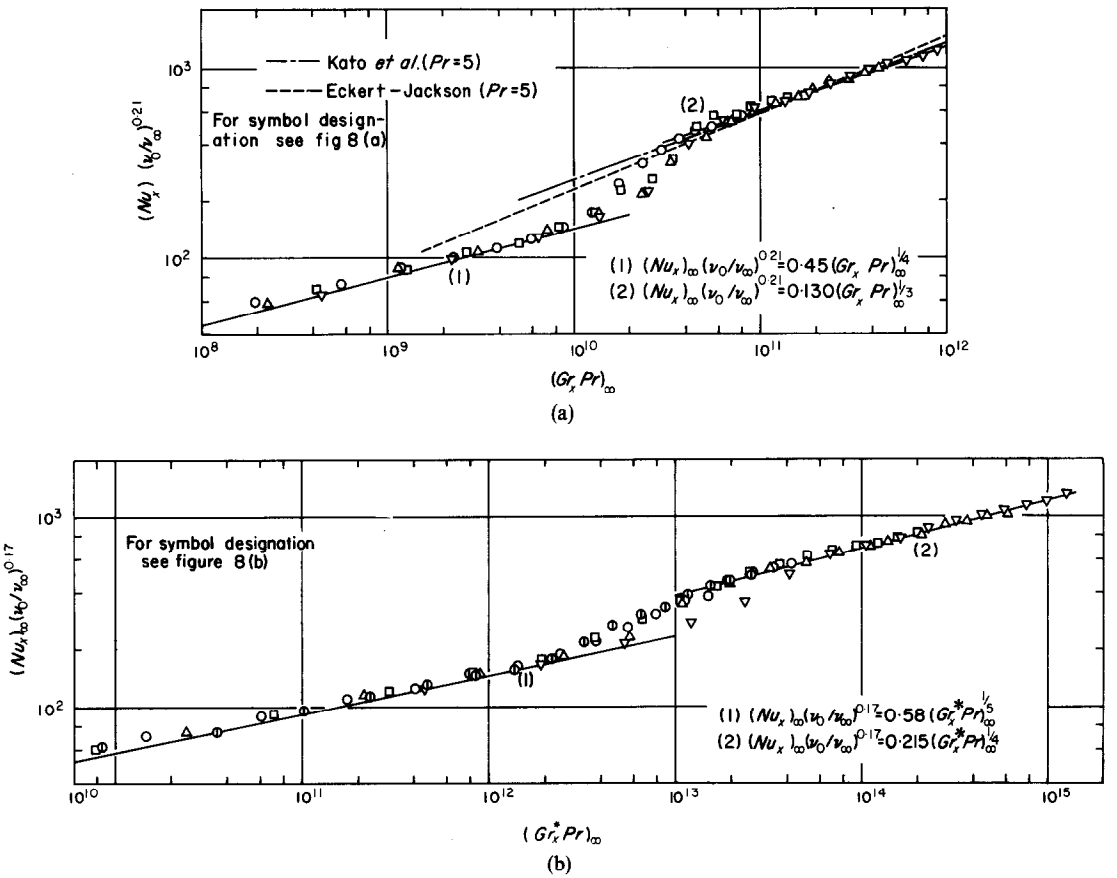

FIG. 11. Non-dimensional correlation of α_x for water. (a) uniform wall temperature. (b) uniform heat flux.

pecially in the case of uniform wall temperature, may be due to the experimental error caused by inappropriate supply of the heat flux. Nevertheless, it is noteworthy that equation (14) holds independently of the kinds of fluid within the range of $(Pr)_e$ from 0·7 to 300.

(v) In the region of the transition from laminar to transition-turbulent region, or to turbulent region with respect to water, local heat transfer coefficients increase abruptly. This narrow region is named "transitional" region. The values of $(Gr_xPr)_e$ corresponding to the range of transitional region vary with the kinds of fluid, and even for respective fluid they are not exactly determined. The transition from transition-turbulent to turbulent region is continuous, and the value of $(Gr_xPr)_e$ corresponding to it is almost definite as far as one kind of fluid is concerned.

(vi) In laminar region the agreement between theoretical and experimental results is good. In turbulent region the theoretical solutions of Kato *et al.* [7] and Eckert and Jackson [8] are inserted as a chain and a dashed line respectively in Figs. 8(a), 9(a) and 10(a). The former agrees well with only the data on water. The latter agrees with the data on spindle oil with respect to only the exponent on $(Gr_xPr)_e$. However, the theoretical solutions for turbulent region are not generally reliable.

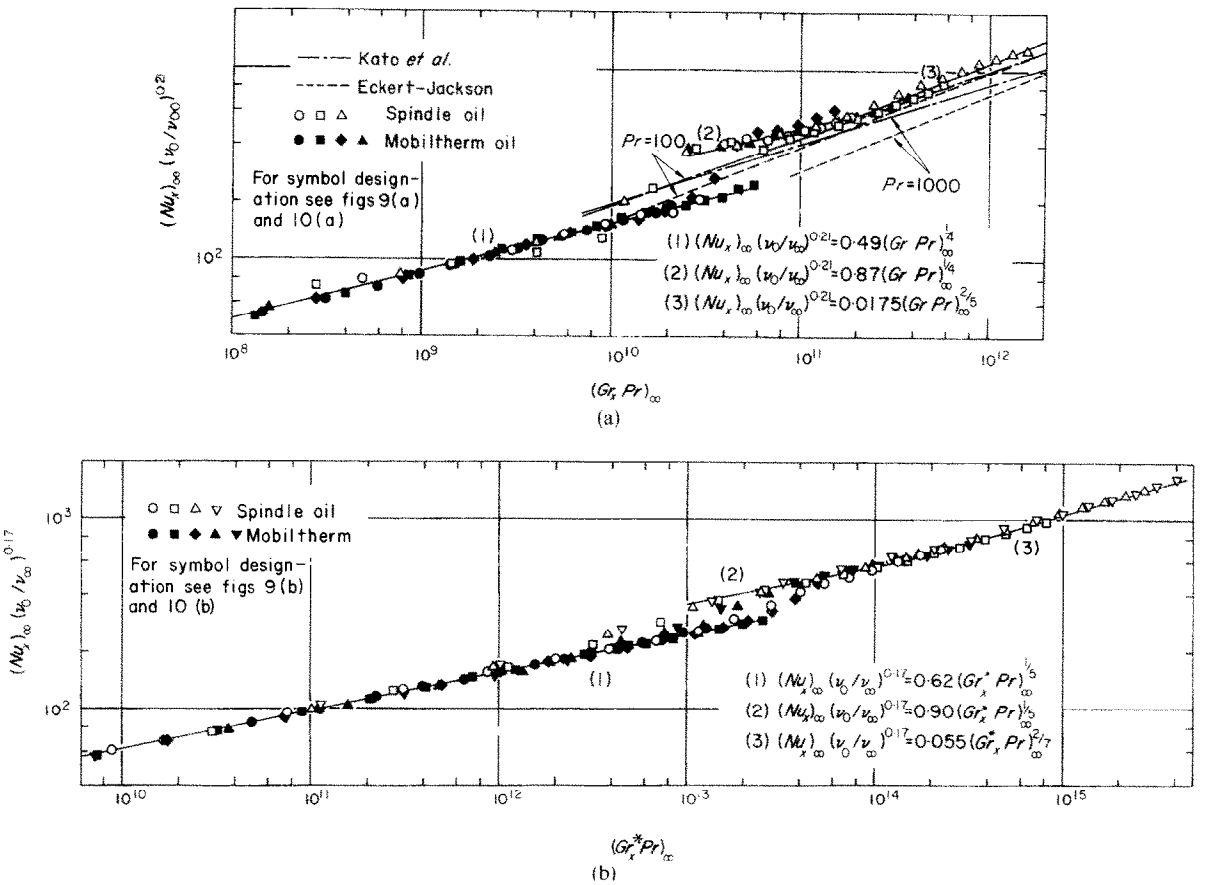

FIG. 12. Non-dimensional correlation of α_x for spindle oil and Mobiltherm oil. (a) uniform wall temperature. (b) uniform heat flux.

4.2 *Non-dimensional expressions of local heat transfer coefficients under consideration of only the variation of viscosity.*

The variation of viscosity with temperature is most conspicuous, therefore we attempt to supplement the nondimensional equations of local heat transfer coefficients by specified values of kinematic viscosity, neglecting the variation of the other properties. Figures 11 (a), (b) and 12 (a), (b) show plots of $(Nu_x)_\infty (v_0/v_\infty)^{0.21}$ vs. $(Gr_xPr)_\infty$ and $(Nu_x)_\infty(v_0/v_\infty)^{0.17}$ vs. $(Gr_x^*Pr)_\infty$ on the same data with the preceding section, where $(\ )_\infty$ signifies that the values of physical properties λ, ν and Pr at t_∞ are employed. The exponent 0·21 of supplementary term (v_0/v_∞) is applied after Akagi's proposition [14] on the expression of the numerical solutions of the laminar boundary layer equations in the case of uniform wall temperature. The exponent 0·17 in the case of uniform heat flux is formally induced by introducing transformation (19) to the above case, namely, $(Nu_x)_\infty(v_0/v_\infty)^{0.21}$ is proportional to $(Gr_xPr)_\infty^{\frac{1}{4}}$. The correlations of the data are as good as those of the preceding section as a whole.

With respect to laminar and turbulent region of water as well as laminar and transition-turbulent region of spindle oil and Mobiltherm oil, the experimental equations obtained in Figs. 11 and 12 are respectively the same as

those derived from the replacement of

$$(Nu_x)_e \rightarrow (Nu_x)_\infty (\nu_0/\nu_\infty)^{0.21}$$

and

$$(Gr_x Pr)_e \rightarrow (Gr_x Pr)_\infty$$

in equations (8), (12), (9) and (14); or

$$(Nu_x)_e \rightarrow (Nu_x)_\infty (\nu_0/\nu_\infty)^{0.17}$$

and

$$(Gr_x^* Pr)_e \rightarrow (Gr_x^* Pr)_\infty$$

in equations (10), (13), (11) and (15).

Moreover, the upper limits of laminar region are expressed by $(Gr_x Pr)_{\infty cri} = (1 \sim 5) \times 10^{10}$ and $(Gr_x^* Pr)_{\infty cri} = (0{\cdot}2 \sim 2.5) \times 10^{13}$, and the lower limits of transition-turbulent region of spindle oil and Mobiltherm oil, or turbulent region of water, are expressed by $(Gr_x Pr)_\infty =$

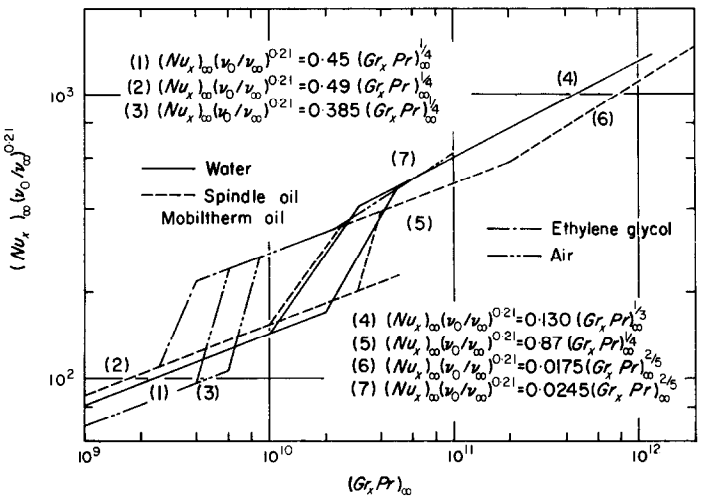

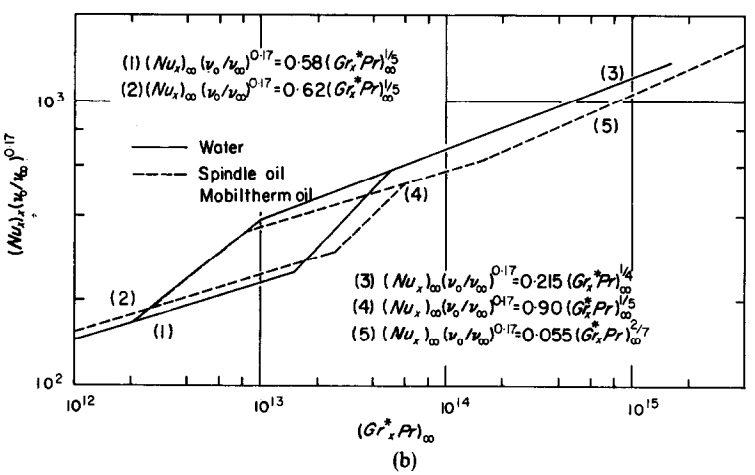

FIG. 13. Comparison on experimental equations of local heat transfer coefficients. (a) uniform wall temperature. (b) uniform heat flux.

$(2{\cdot}5 \sim 6) \times 10^{10}$ and $(Gr_x^* Pr)_\infty = (1 \sim 5) \times 10^{13}$. The fact that the lower and upper limits of transitional region expressed as above are independent of the kinds of fluid, suggests that these transition phenomena are subject to the flow of relatively outer part in the boundary layer.

The experimental equations for turbulent region of spindle oil are expressed as follows:

$$(Nu_x)_\infty (v_0/v_\infty)^{0{\cdot}21} = 0{\cdot}0175\,(Gr_x Pr)_\infty^{\frac{2}{3}}, \quad 2{\cdot}0 \times 10^{11} \leqslant (Gr_x Pr)_\infty ; \qquad (20)$$

and

$$(Nu_x)_\infty (v_0/v_\infty)^{0{\cdot}17} = 0{\cdot}055\,(Gr_x^* Pr)_\infty^{\frac{1}{4}}, \quad 1{\cdot}5 \times 10^{14} \leqslant (Gr_x^* Pr)_\infty . \qquad (21)$$

With respect to the coefficients and the ranges of application, these equations are different from those of equations (16) and (17) respectively.

The exponents of supplementary term (v_0/v_∞) in the experimental equations in this section have not been induced theoretically except for the laminar region in the case of uniform wall temperature, but we can practically take 0·21 in the case of uniform wall temperature and 0·17 in the case of uniform heat flux, commonly over the range from laminar to turbulent region. Moreover, the characteristics of the local heat transfer coefficients obtained in the preceding section hold as they are, and the expressions on the range of transitional region are made much simpler.

Figure 13 (a) shows all of the experimental equations obtained in this section in the case of uniform wall temperature. In this figure, are also described the curves of the experimental equations derived from Fujii's data [1] for heat transfer from a vertical cylinder to ethyleneglycol and given by Cheesewright [4] from a vertical plate to air.

It is recognised that the values of $(Gr_x Pr)_{\infty \mathrm{cri}}$ corresponding to the upper limit of laminar region vary with experimental apparatuses. Besides, in Saunders' experiments of heat transfer from a vertical plate to air [17] and to water [18], the values were about $(2 \sim 3) \times 10^9$. Generally, the values of $(Gr_x Pr)_{\infty \mathrm{cri}}$ on a vertical plate are smaller, because the occurrence of these transitions is closely connected to the stability of the laminar boundary layer flow. In this case two-dimensionality of the boundary layer is disturbed directly owing to side-wise entrainment of fluid on the plate and indirectly owing to simultaneous lowering of wall temperature near the side edges. That the experiments of Cheesewright [4] show the higher values of $(Gr_x Pr)_{\mathrm{cri}}$, may be due to the fact that side-wise entrainment of fluid on the plate was precluded in his apparatus.

Figure 13 (b) shows all of the experimental equations obtained in this section in the case of uniform heat flux. The values of $(Gr_x Pr)_\infty$ and $(Gr_x^* Pr)_\infty$ corresponding to transitional region are also mutually transformed by equation (19) in case of similar conditions in the ambient, which are mentioned in section 4.7.

4.3 *Average heat transfer coefficients*

Average heat transfer coefficients are expressed nondimensionally in the case of uniform wall temperature. Average Nu number and Gr number based on height L are respectively defined by

$$Nu_L = \frac{\alpha_L L}{\lambda} = \frac{1}{\lambda}(t_0 - t_\infty) \int_0^L q \, \mathrm{d}x, \qquad (22)$$

$$Gr_L = \frac{L^3 g \beta (t_0 - t_\infty)}{\nu^2}. \qquad (23)$$

The correlations of Nu_L vs. Gr_L can be calculated from the respective equations on Nu_x obtained in section 4.1. and 4.2. In laminar region they naturally coincide with the theoretical solutions. When the integrand of equation (22) involves two or three regions, the induced equations are affected by the heights of occurrence of the transitions. Therefore, we propose the equations with an indefinite constant in order to cover all experimental data on each fluid, in accordance

with the expressions obtained in section 4.2. as follows:

for water,

$$(Nu_L)_\infty(v_0/v_\infty)^{0.21} = 0.130\,(Gr_L Pr)_\infty^{\frac{1}{3}} - (111 \sim 176), (1.5 \sim 4) \times 10^{10} \leqslant (Gr_L Pr)_\infty; \quad (24)$$

for spindle oil and Mobiltherm oil, commonly,

$$(Nu_L)_\infty(v_0/v_\infty)^{0.21} = 1.16\,(Gr_L Pr)_\infty^{\frac{1}{4}} - (177 \sim 227), (1.5 \sim 4) \times 10^{10} \leqslant (Gr_L Pr)_\infty \leqslant 2.0 \times 10^{11}; \quad (25)$$

$$(Nu_L)_\infty(v_0/v_\infty)^{0.21} = 0.0145\,(Gr_L Pr)_\infty^{\frac{2}{5}} + (115 \sim 65), 2.0 \times 10^{11} \leqslant (Gr_L Pr)_\infty. \quad (26)$$

In order to simplify the calculation in the above equations, the variations of heat transfer coefficients in transitional region are left out of account. Namely, it is assumed that these transitions take place discontinuously at the points of lower limits of $(Gr_L Pr)_\infty$ indicated under equations (24) and (25). The ranges of the constants in the right side of equations (24)–(26) correspond to the range of $(Gr_L Pr)_\infty$ at those hypothetical transition points.

In order to correlate the experimental data, it suffices to use the definitions (22) and (23) as $\int_0^i g\,dx = \sum_{i=1}^{i} g_i$ and $L = x_j$. As to q_1, however, are used the calculated values from the experimental equation of $(Nu_x)_\infty$, because the measured values with respect to this subdivided section include conductive heat losses. The ambient fluid temperature on a level at $0.15L$ from the lower end of the heated cylinder is taken as the effective temperature. This value was proposed by Yamagata and Kawano [19] theoretically and assured by Fujii [1] experimentally. It is applicable only to laminar convection, but not to the convection including turbulent region. For the data in this paper, however, the selection of the level corresponding to the effective temperature is little important, because temperature gradients in the ambient are comparatively small to the difference between t_0 and t_∞.

The data shown in Fig. 14, which are chosen by two test runs with most different values of $(Gr_x Pr)_{\infty cri}$ for each fluid, are in good agreement with the predicted equations (24)–(26) respectively. In this figure, are also inserted correlation curves of air by Cheesewright [4] and of

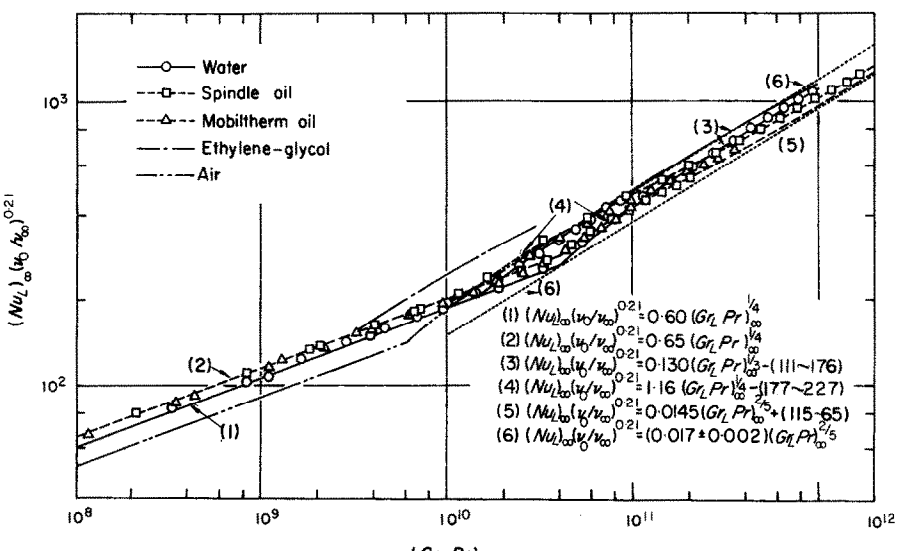

FIG. 14. Experimental data and its correlations on average heat transfer coefficients in the case of uniform wall temperature.

ethylene-glycol by Fujii [1], both of which are derived by integration of the local heat rates.

The above-mentioned data on water, spindle oil, Mobiltherm oil and air may be uniquely correlated in the range of $(Gr_L Pr)_\infty$ larger than 10^{10} by the following equation:

$$(Nu_L)_\infty (v_0/v_\infty)^{0.21} = (0.017 \pm 0.002) \times (Gr_L Pr)_\infty^{\frac{1}{4}}, \quad 10^{10} \leqslant (Gr_L Pr)_\infty. \tag{27}$$

This equation is useful to estimate approximately average heat transfer coefficients, but it cannot correctly correlate the data of each individual test run. It must not be applied, when the upper limit of laminar region becomes much smaller, as shown by the curve of ethylene-glycol in Fig. 14. Touloukian *et al.* [20] also proposed an experimental equation applicable to the data on water and ethylene-glycol, but it is different from equation (27) in both trend and magnitude. Their results are rather unreliable, because the number of subdivision of the heated cylinder was too few and the effective fluid temperature above-mentioned was taken inappropriately.

4.4 *Flow patterns and transition phenomena*

Mirage photos of the boundary layer of spindle oil are shown in Fig. 15, photos (a) and (b) of which correspond to the cases of comparatively small and large heat flux respectively. Since each of them was taken partially and then pieced together, simultaneity along the height of the cylinder is not provided.

The laminar layer is built up from the leading edge. At about $(Gr_x^* Pr)_\infty \approx (4{,}1{\cdot}5) \times 10^{12}$, pairs of inward and outward rotational motion are gradually developed. Successively, in the region of $(6, 3) \times 10^{12} \lesssim (Gr_x^* Pr)_\infty \lesssim (2{\cdot}5, 1{\cdot}1) \times 10^{13}$, vortex pairs are formed up and arranged in the formation of a symmetrical double row. This layer is named "vortex-street layer". The ranges of $(2{\cdot}5, 1{\cdot}1) \times 10^{13} \lesssim (Gr_x^* Pr)_\infty \lesssim 1{\cdot}5 \times 10^{14}$ and $1{\cdot}5 \times 10^{14} \lesssim (Gr_x^* Pr)_\infty$ correspond to transition-turbulent and turbulent region respectively, which are defined in previous sections from the results of non-dimensional correlations of heat transfer coefficients. The limits of each flow patterns are not clearly defined and their locations also somewhat vary with time. The indicated values of $(Gr_x Pr)_\infty$ and $(Gr^* Pr)_\infty$ corresponding to their limits, however, are scarcely affected by the amount of temperature or heat flux on the heated cylinder.

Successive photos of a vortex-pair in Fig. 16 were taken by following up the process of its development, disintegration and transition to transition-turbulent with a movie camera. Each photo is extracted by 1/4 s interval, and black and white is reversed. Moreover, it should be noted that no behavior of the fluid outside the thermal boundary layer appeared in the photos because of uniform temperature.

According to the observation based on statical coordinate as shown in Fig. 15, the flow pattern indicated by the photos from No. 0 to No. 3 in Fig. 16 looks like a wave motion, and Eckert and Soehngen [8] suggested from their interferometric observation on air that the waves resembled closely the Tollmien-Schlichting wave in a forced flow boundary layer. Each individual fluid particle in the boundary layer, however, never fluctuates. On the other hand, the travelling velocity is dependent on the main flow velocity but not on the physical properties of the medium. Therefore, this fluid motion must be distinguished from ordinary wave motion.

In No. 4 of Fig. 16 inversion of stripes is found, and successively a clear shape of vortex-pair appears. This vortex-pair corresponds with what was conceived theoretically by Fujii [10,21] from his shadow graphs of the boundary layer of ethyleneglycol and confirmed by Szewczyk [9] from the observation of dye streaks injected in the boundary layer of water. While the outside vortex is pushed outward, the ambient fluid with low temperature is engulfed into the wake of the vortex. Accordingly, the thickness of the thermal boundary layer at this portion between two vortex-pairs becomes thinner than that at just upstream in the ordinary laminar

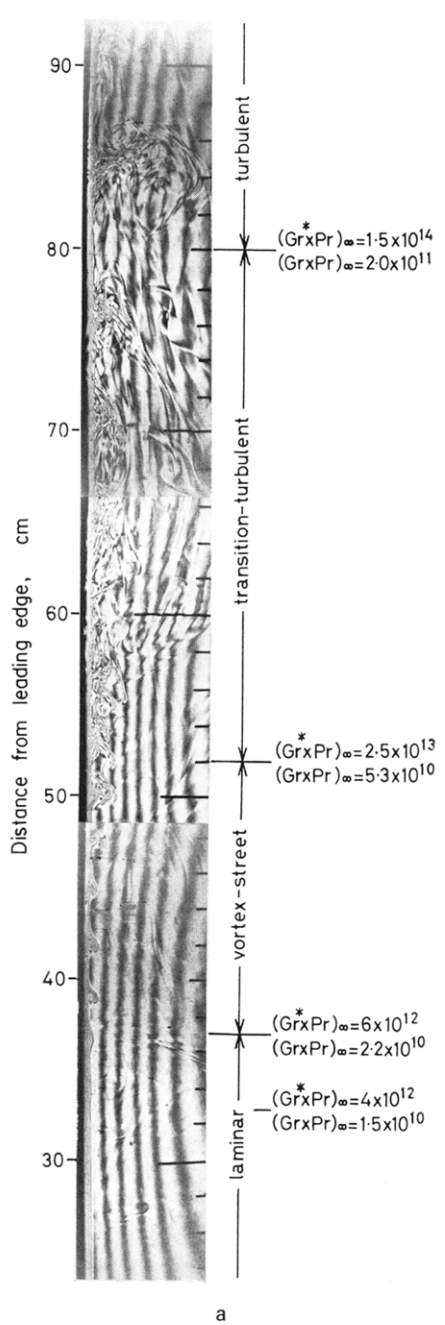

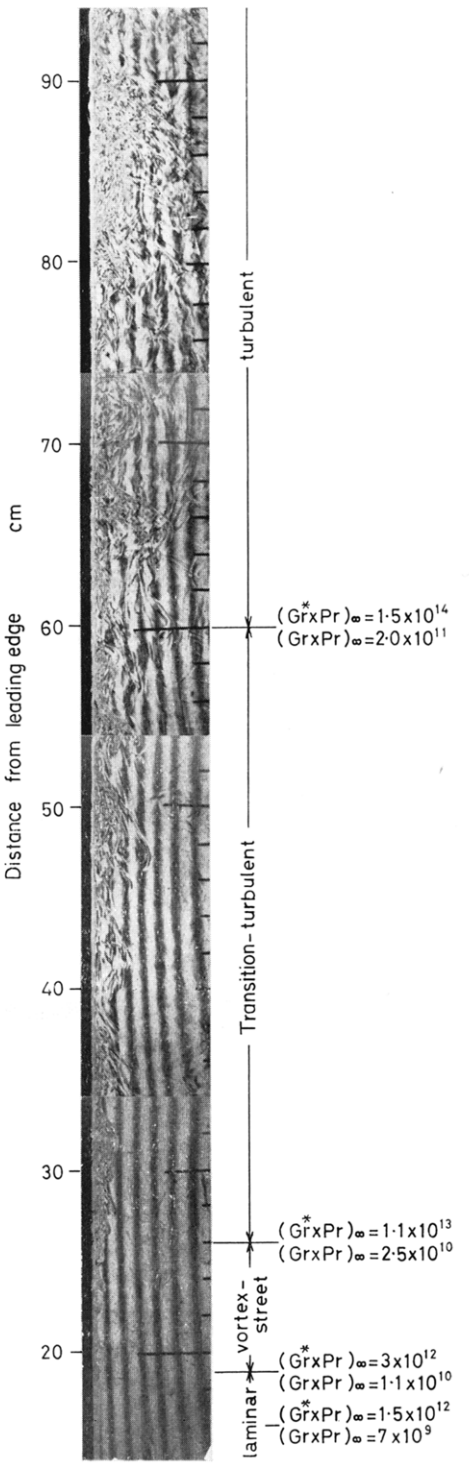

FIG. 15. Mirage photos of the boundary layer of spindle oil.
(a) smaller heat flux; $q = 3{\cdot}86 \times 10^3$ W/m^2.
(b) larger heat flux; $q = 1{\cdot}23 \times 10^4$ W/m^2.

facing page 770

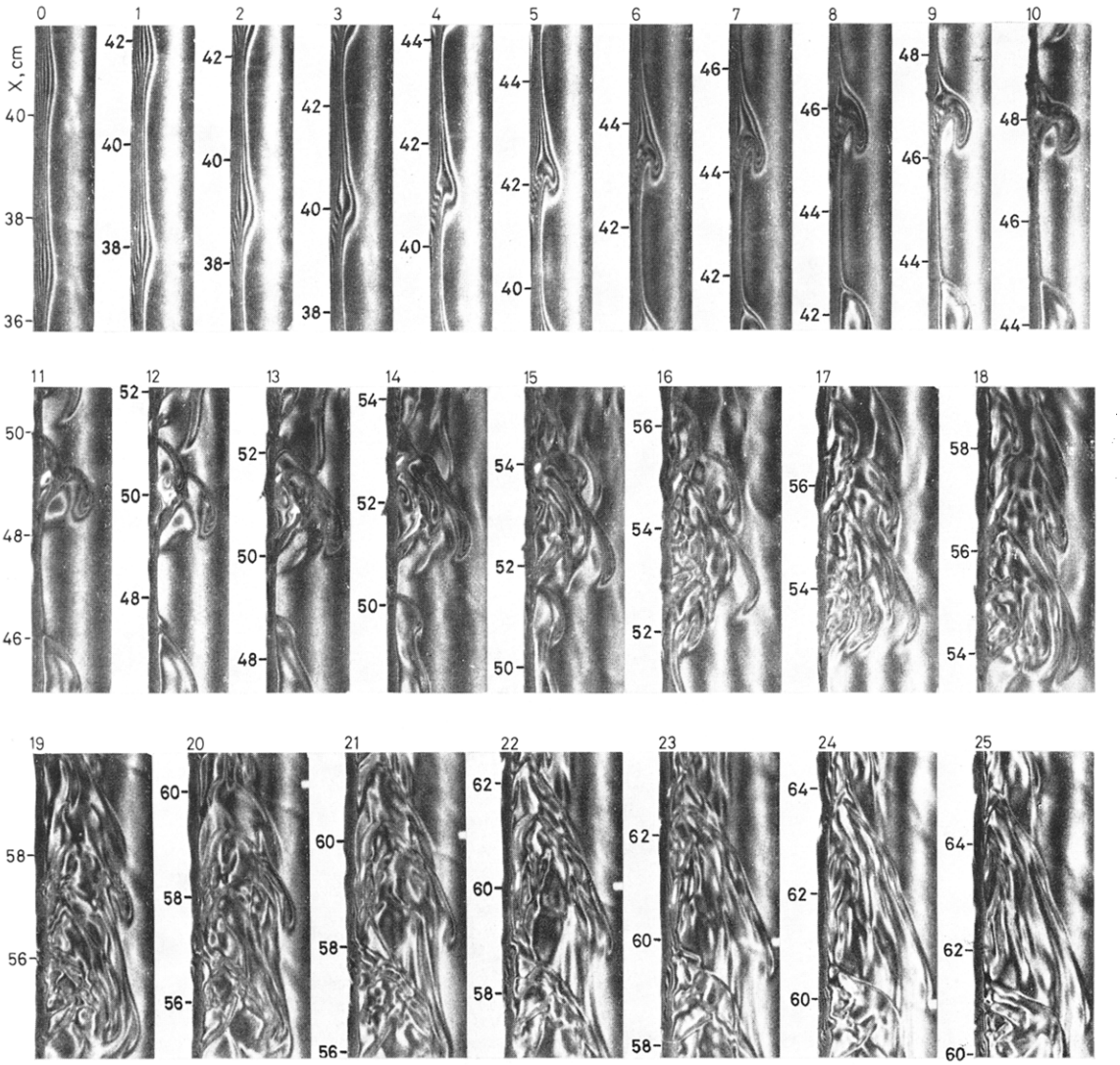

FIG. 16. Successive photos of a vortex pair of spindle oil; intervals of each photos is 1/4 s, $q = 3{\cdot}86 \times 10^3$ W/m^2. $(Gr_x^* Pr)$w $= 1{\cdot}15, 3{\cdot}96 \times 10^{13}$ at $x = 42, 57$ cm respectively.

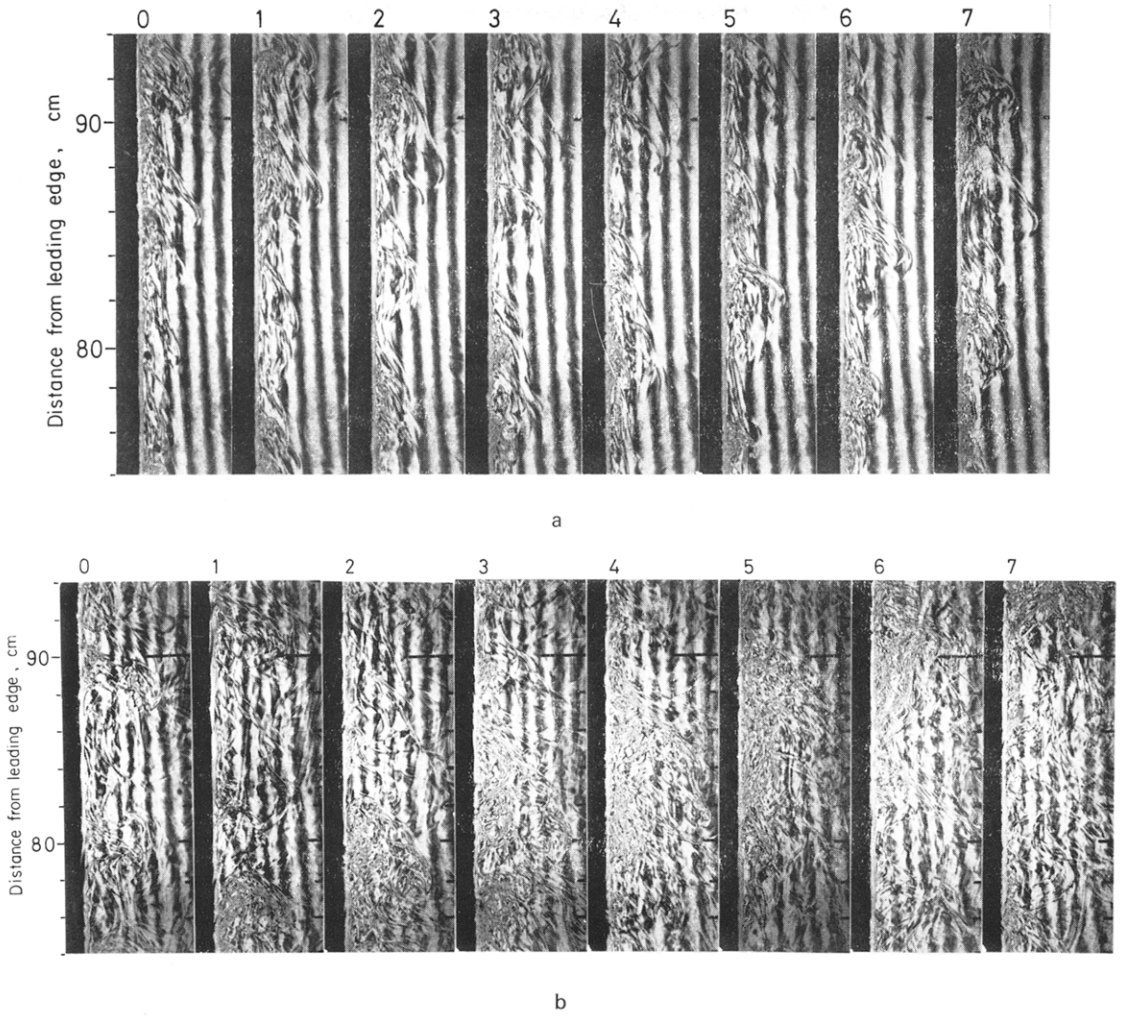

FIG. 17. Comparison between the transition–turbulent and turbulent flow pattern of spindle oil; interval of each photo is 1/2 s, $q = 1{\cdot}23 \times 10^4$ W/m^2.

(a) transition–turbulent; $(Gr_x^* Pr)_\infty = 7{\cdot}76 \times 10^{13}$ at $x = 42$ cm.

(b) turbulent; $(Gr_x^* Pr)_\infty = 1{\cdot}15 \times 10^{15}$ at $x = 82$ cm.

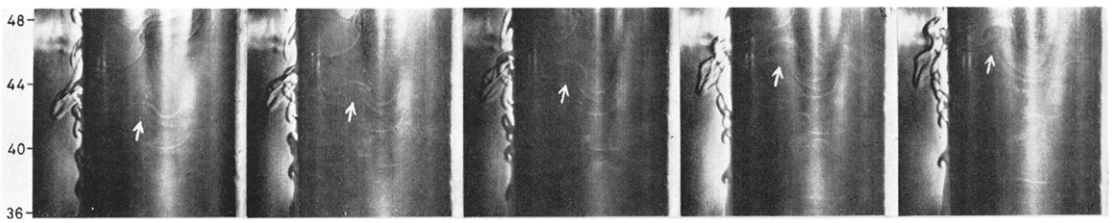

FIG. 18. Deformation of the vortices observed from the front of the heated cylinder; $q = 3{\cdot}86 \times 10^3$ W/m^2, $(Gr_x^* Pr)_x$ $0{\cdot}94, 1{\cdot}90 \times 10^{14}$ at $x = 40, 48$ cm respectively.

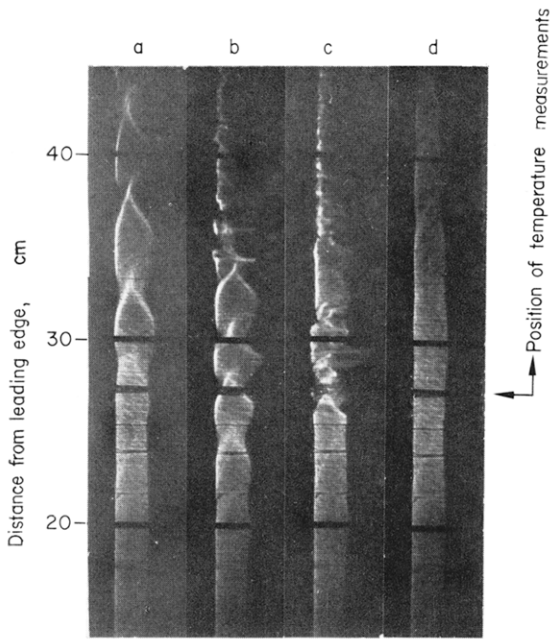

FIG. 30. Shadow graphs of the transitional region of water.

boundary layer. The flow pattern from No. 4 to No. 13 corresponds to vortex-street layer, and this region corresponds to transitional region in the curve of $(Nu_x)_\infty$ vs. $(Gr_x^* Pr)_\infty$.

The flow pattern from No. 13 to No. 25 of Fig. 16 corresponds to transition-turbulent region. The shape of vortices first disintegrates and the fluid part with irregular turbulent motion gradually extends in the boundary layer. In the part close to the heated cylinder, however, remains a thin layer with comparatively less turbulence, which may be taken as the laminar sub-layer.

In Fig. 17, for comparing the transition-turbulent flow (a) with the turbulent flow (b), are represented the mirage photos, which are in the same condition as Fig. 15(b) and are taken by every $\frac{1}{2}$ s. In the part that active turbulent mixing occurs, the stripes change into specks, and the more active the mixing, the smaller and the more randomly situated the specks. It is recognized that the part with active turbulence rises in a lump. The size of the lump is at first small in the transition-turbulent region and gradually increases, whereas in the turbulent region it is comparatively large and varies little. When the lumps pass, the part close to the heated cylinder, that is called laminar sub-layer, is also disturbed violently.

Figure 18 shows the deformation of vortices, which are found when the front of the heated cylinder is illuminated from above the observer. Glimmering lines accompanied with a black line beneath them indicate outer vortices in the boundary layer. Because the outer vortex is made of the fluid with relatively small refractive index compared to the neighbourings, a reflective surface against injected light beams is formed on the vortex tube, and the part behind the reflected light on the heated cylinder is shaded. On the left side of the heated cylinder in the figure is also shown the boundary layer illuminated by a lamp settled behind the heated cylinder.

The vortex tube surrounds the heated cylinder in a ring. The axis of the tube is not just perpendicular to the flow direction in its starting. This suggests that the conditions of vortex development and the flow velocity in the laminar layer are not just uniform circumferentially. When the translation velocity of the vortex tube is larger than the mean velocity of its neighbourings, the vortex is subject to a force pushing itself outward, based on the Kutta–Joukowsky theorem. As the vortex tube is transferred outward, it is further pushed outward and its vertical velocity component decreases, since the above-mentioned relative velocity becomes larger.

The vortex tube, however, does not uniformly expand outward, but its some parts are retarded outward and advanced vertically. This stage is indicated by some bended lines in Fig. 18 and by disintegrated stripes in mirage photos Nos. 10–13 of Fig. 16. The bended part is more and more accelerated and its foremost round end becomes larger. Precisely, the bended part forms a loop, the legs of which are connected to relatively outward located parts of the same vortex tube and the head of which is inclined inward. The loop expands rapidly as if it gets beneath the preceding vortex tube, while the part of this tube is more impressed outward, and diffused out in the ambient as if a free vortex tube. By analogical inference from the character of vortices in an inviscid fluid, it is explained that the loop must be accelerated by all the forces exerted from the mutual reactions among the vortices arranged along the flow, between the vortices and the cylinder wall and between the vortices and the surrounding flow. While the loop is elongated and its head is expanded, the ambient fluid is engulfed into its wake three-dimensionally. This part corresponds to a turbulent lump in Fig. 17.

Inner vortices must be more stable, because they are close to the heated cylinder and therefore subject to an intense viscous force. Their motion however were not clarified. It is reasonable to infer that the inner vortices play a certain important role in the transition of flow patterns and the promotion of turbulent mixing, because they are developed together with outer vortices in

symmetrical arrangement, and they must intersect or come into collision with the loops of outer vortices.

As the vortices are deformed, the fields of flow and temperature or buoyancy are disturbed, and inversely the disturbed fields promote further the deformation of vortices, therefore, under these reciprocal action the flow becomes more and more irregular. That turbulence becomes drastic, is equivalent to that apparent thermal conductivity of the fluid becomes large, therefore heat transfer coefficients are enhanced. In the stage of disintegration of the vortex-street, notwithstanding the flow is not turbulent, the heat transfer coefficients increase very rapidly. Its cause may be that the disintegrated vortex tubes engulf the ambient fluid into the boundary layer three-dimensionally. The similar activities may be maintained in the turbulent lumps too.

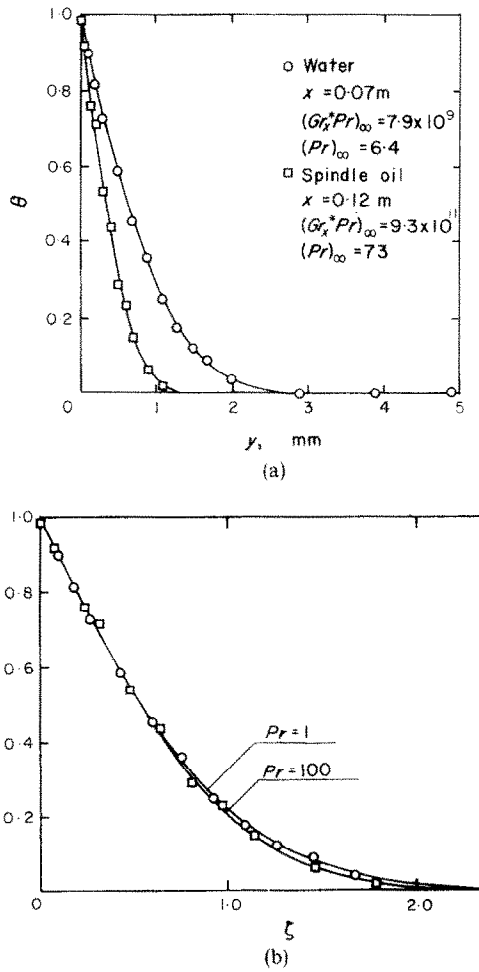

FIG. 19. Temperature profiles in the laminar boundary layer. (a) measurements. (b) non-dimensional expressions and theoretical curves as $Pr = 1$ and 100.

In transition-turbulent region, heat transfer coefficients decrease as distance x increases. Its cause may be that the time-mean thickness of the boundary layer grows with relatively large rate, therefore, that the time-mean velocity grows with relatively small rate. In turbulent region, on the other hand, heat transfer coefficients increase as distance x increases. This characteristic cannot be extrapolated to very large Gr number without reservation, since the laminar sub-layer must become infinitely thinner according to conventional approximate theories. Furthermore, the turbulent boundary layer revealed in this paper is not so homogeneous as has been conceived in theoretical studies.

For the boundary layer of water no typical processes as above were observed, however, it may be appreciated that the fundamental mechanism of the phenomena is similar.

It is guessed that the boundary layer along a vertical plate becomes more unstable, since a vortex tube must be endless essentially and its shape is affected by the configuration of the plate especially in its side edges. In this case, correspondingly, the upper limit of the laminar boundary layer is much lower.

4.5 *Temperature field in the boundary layer*

The results of temperature measurements in the laminar boundary layer are shown in Fig. 19(a), where non-dimensional temperature $\theta = (t - t_\infty)/(t_0 - t_\infty)$ is taken to ordinate and distance y from the heated cylinder to abscissa, t is the temperature at point y and t_0 the wall temperature, which was measured by the thermocouple inserted in the heated cylinder.

Thickness of the thermal boundary layer δ is defined as the value of y at which the tangent of the temperature profile at $y = 0$ crosses with

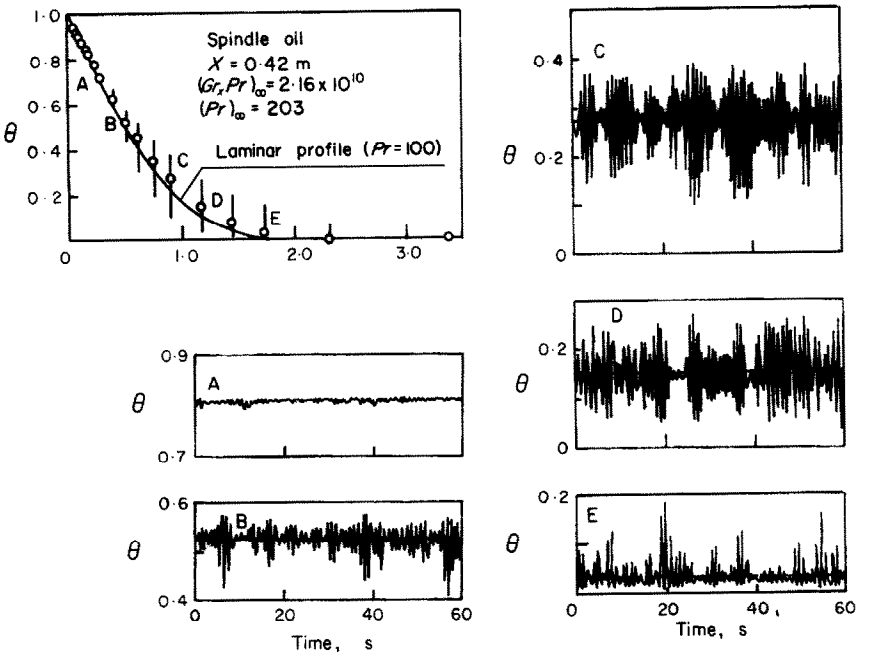

FIG. 20. Records of the temperature fluctuations in the vortex-street layer of spindle oil.

axis y. Thus defined δ is shown to be that

$$\delta = \frac{x}{Nu_x}. \tag{28}$$

Then, correlation variable ζ is introduced as

$$\zeta = \frac{y}{\delta} = \frac{y}{x} Nu_x. \tag{29}$$

The data of Fig. 19(a) is normalized by equation (29) and shown in Fig. 19(b), together with the theoretical results for $Pr = 1$ and 100 [15]. This figure exhibits that the measurements are reliable and the correlation variable is desirable.

Figures 20 and 21 show the records of temperature fluctuations in the vortex-street and turbulent layer of spindle oil respectively, where the temperatures are normalized for convenience of comparison. Although the fluctuations are irregular, we can evaluate the time-mean temperature from such a record over an adequate period. The evaluation was at first performed by a curve tracer and an analogue integrator, and otherwise the average line was drawn on the record by eye-criterion. Since discrepancy of the results by these both evaluations was of the same order of magnitude as the accuracy of temperature measurements, the majority of the data was treated by the latter. Thus the time-mean temperature profiles were obtained and shown in Figs. 20 and 21. The vertical bars on each curve indicate the largest amplitudes of the respective records.

The records in Fig. 20 exhibit that the fluid lumps of lower or higher temperature come into the places located closer to or farther from the heated cylinder respectively, for a short time interval with a certain period, and it is most representative at point (B) or (E). Furthermore, the period coincides with the generation period of a vortex-pair. These facts are suggestive of the correspondence of one wave on the record to one vortex-pair. In Fig. 21, the wave form is disintegrated and the apparent period is somewhat long, compared with the case of vortex-street. From an analogical inference based on

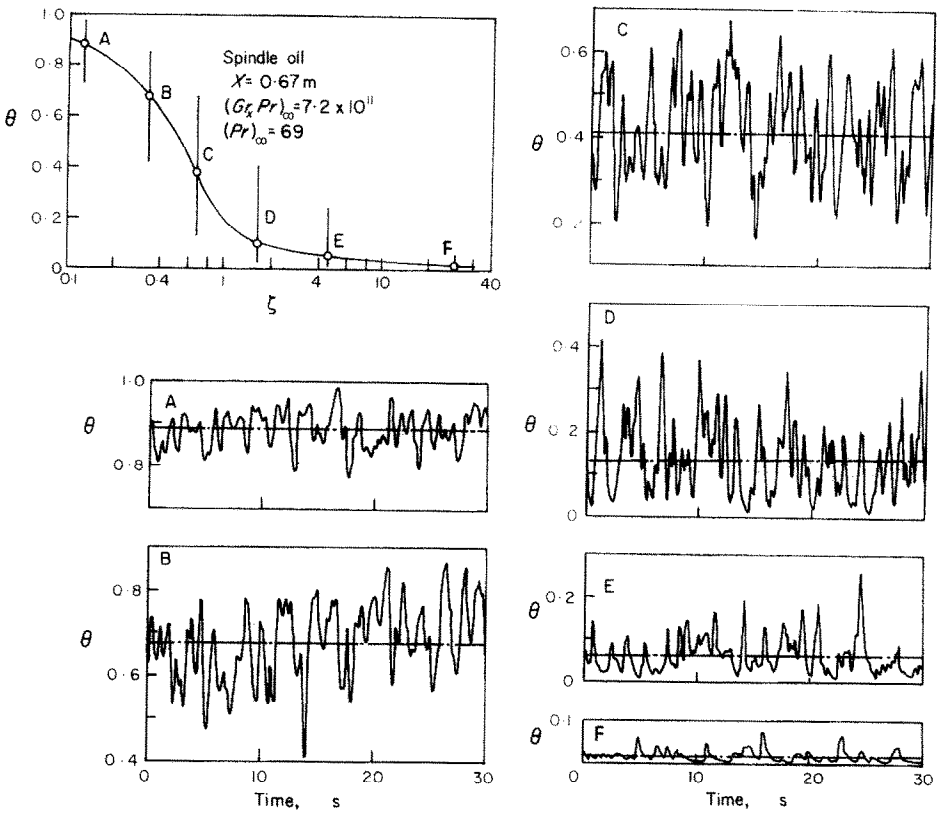

FIG. 21. Records of the temperature fluctuations in the turbulent layer of spindle oil.

the explanation of Fig. 20 and from the results of observations shown in section 4.4, the crests and troughs of the waves in Fig. 21 may be ascribed to the passage of the turbulent lumps. The records for transition-turbulent region resemble those for turbulent, except for the fact that the amplitude of temperature fluctuations is comparatively small.

All instances of the measurements of the time-mean temperature profiles and the maximum amplitudes under widely different experimental conditions are shown in Fig. 22 for turbulent region of water, in Figs. 23 and 24 for transition-turbulent and turbulent region of spindle oil respectively. It is appreciated from these figures that good correlations of time-mean temperature profiles are achieved by means of the non-dimensional temperature and the correlation variable defined by equation (29). In other words, if the non-dimensional demonstration of the data is carried out so that the temperature gradients close to the heated cylinder are brought to accord, the temperature profiles over the whole range of y-direction are naturally brought to accord. The amplitude of temperature fluctuations of water is comparatively large whereas that of spindle oil is comparatively small. Especially in transition-turbulent region, it is much smaller. Since temperature profiles in the range of $0 < \zeta < 0{\cdot}5$ are almost linear, this range may be regarded as the laminar sub-layer, but in it also fairly large temperature fluctuations are measured.

Simple and rough representations of time-

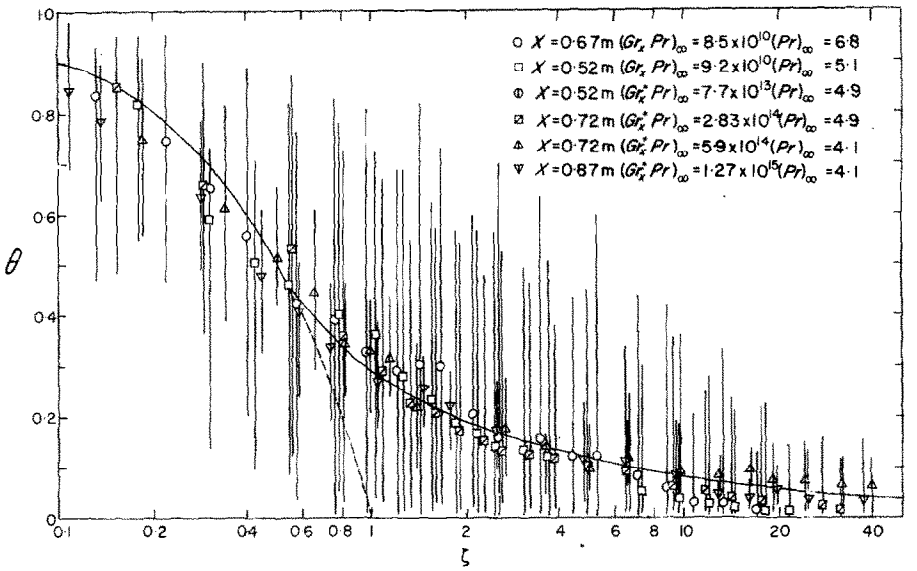

FIG. 22. Time-mean temperature profile and maximum temperature amplitudes in the turbulent layer of water.

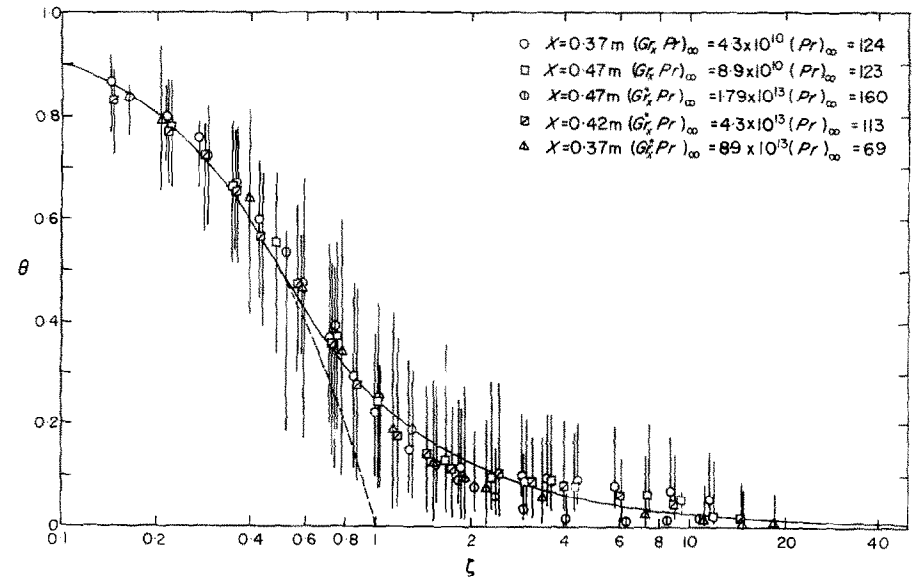

FIG. 23. Time-mean temperature profile and maximum temperature amplitudes in the transition-turbulent layer of spindle oil.

mean temperature profiles are proposed as follows:

for water,

$$\theta = 1 - \zeta, (0 < \zeta < 0{\cdot}5),$$

$$\theta = \frac{0{\cdot}25}{(\zeta - 0{\cdot}25)^{\frac{1}{4}}}, (\zeta > 0{\cdot}5); \tag{30}$$

for spindle oil,

$$\theta = 1 - \zeta, (0 < \zeta < 0{\cdot}5),$$

$$\theta = \frac{0{\cdot}25}{\zeta},)\zeta > 0{\cdot}5). \tag{31}$$

It is worthy to remark that the non-dimensional temperature profile of spindle oil is represented by the same equation for both cases of transition-turbulent and turbulent region, though ζ for each case is defined by the different function of Gr_x or Gr_x^*. The same fact is valid also for the time-mean temperature and velocity profile of air obtained by Cheesewright [4]. For instance, the temperature profile is expressed as:

$$\theta = 1 - \zeta, (0 < \zeta < 0{\cdot}2),$$

$$\theta = \frac{0{\cdot}415}{(\zeta^{\frac{3}{2}} + 0{\cdot}18)^{\frac{1}{3}}}, (\zeta > 0{\cdot}2). \tag{32}$$

Equations (30)–(32) are shown altogether in Fig. 25. Unlike the case of laminar region, the variation with Pr number is recognized. Warner and Arpaci [22] concluded that the natural coordinate y was perhaps the most adequate similarity variable for the turbulent case. This variable, however, is available only for the special case such as the heat transfer coefficient is almost independent of Gr_x, to which case their experiments corresponded. In Fig. 25 are also described the profiles adopted by Fujii [3] in his approximate analysis. Although there is a large discrepancy between them and the measured values, the range of the laminar sub-layer suggested theoretically and that of the linear portion of the measured profiles are almost in agreement.

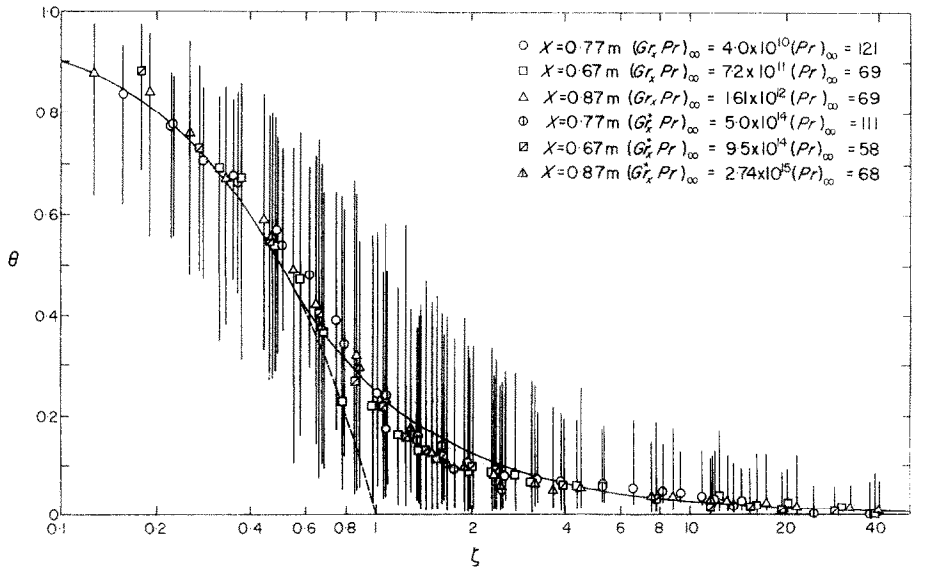

FIG. 24. Time-mean temperature profile and maximum temperature amplitudes in the turbulent layer of spindle oil.

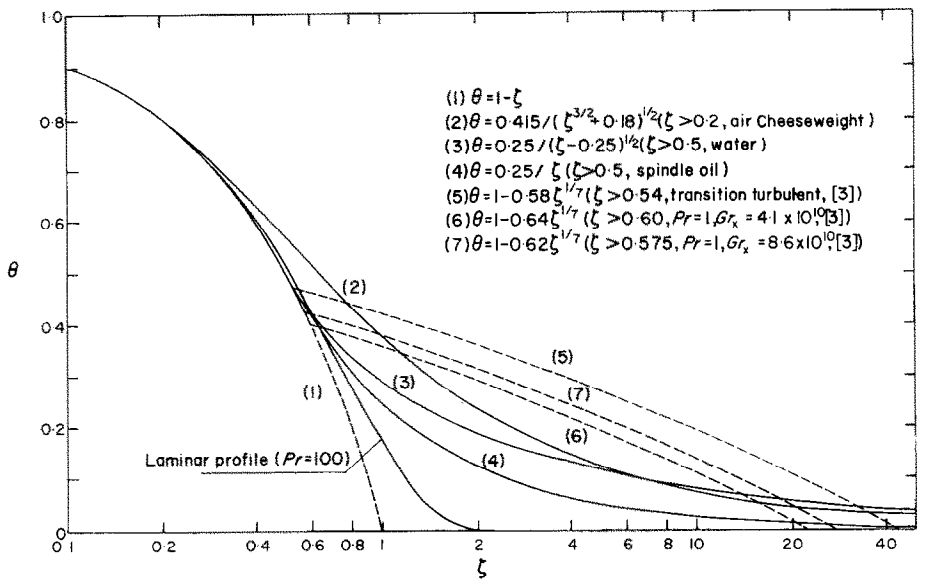

FIG. 25. Comparison on time-mean temperature profiles in the turbulent layer of the various kinds of fluid.

4.6 *Temperature fluctuation of the heated cylinder and its influence upon heat transfer coefficients*

In the case of heat transfer to water, amplitudes of temperature fluctuation of the heated cylinder were particularly conspicuous as shown in Fig. 26. A plot of ratio $\Delta(t_0 - t_\infty)/(t_0 - t_\infty)$ vs. $(Gr_x Pr)_e$ is made from such a record over a period from ten to twenty minutes as shown in Fig. 27, where $\Delta(t_0 - t_\infty)$ is the difference between the maximum and minimum temperature of the heated cylinder and $(t_0 - t_\infty)$ the time-mean temperature difference between the heated cylinder and the ambient. The amplitudes of the fluctuations increase rapidly in transitional region and they are reduced to a certain width in turbulent region. The periods of the fluctuations, which are indicated with some uncertainty in Fig. 28, may be estimated to be several hundred times longer than those with which a vortex-pair is generated. For spindle oil and Mobiltherm oil, the ratio $\Delta(t_0 - t_\infty/(t_0 - t_\infty)$ was smaller than 0·01 and no specially amplified region was found.

Figure 29 indicates the influence of the

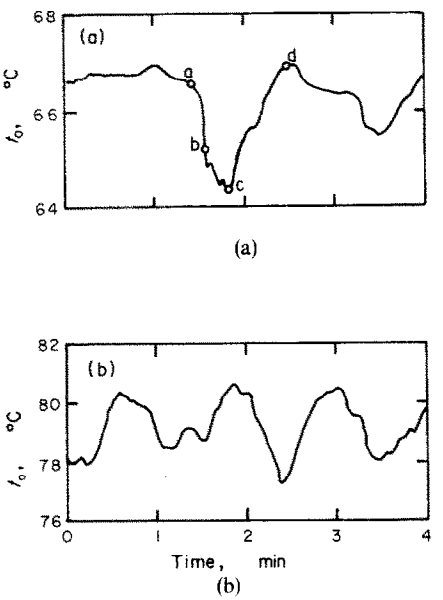

FIG. 26. Temperature fluctuation of the heated cylinder in water. (a) transitional region; $(Gr_x^* Pr)_\infty = 5{\cdot}70 \times 10^{12}$ at $x = 27$ cm.[11] (b) turbulent region; $(Gr_x Pr)_\infty = 4{\cdot}38 \times 10^{11}$ at $x = 67$ cm.

temperature fluctuations of the heated cylinder upon the values of $(Nu_x)_e$ and $(Gr_xPr)_e$. The slanted bars in the figure are obtained by connecting the points corresponding to the maximum and minimum temperatures determined as above. Since these are calculated from the measured values, the actual amplitudes of the wall temperatures must be somewhat larger, and therefore the slanted bars somewhat longer. It is found from this figure that the heat transfer cumferential variation of these phenomena must be taken into account.

It is appreciated that the temperature fluctuation as above is due to indeterminate character of the flow pattern in the transitional region. The vortex-street in the boundary layer is originally unstable and tends to collapse, and in just downstream of the collapse, the heat transfer coefficient increases abruptly. If the heat capacity of the heated cylinder or plate is

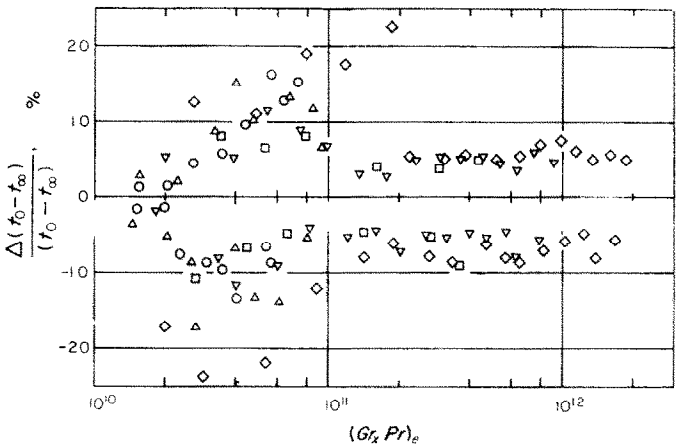

FIG. 27. Amplitudes of the temperature fluctuation of the heated cylinder in water.

coefficients in transitional region fluctuate between those in laminar and turbulent region.

Shadow graphs of transitional region is shown in Fig. 30, where figures (a), (b), (c) and (d) correspond to points a, b, c and d in Fig. 26(a) respectively. When the temperature of the heated cylinder becomes low, the position at which vortex-pairs collapse shifts downward and the flow at the point of temperature measurement is turbulent. On the contrary, when the temperature rises high, laminar flow dominates the measuring position. The period of change of the position at which vortex-pairs collapse is almost in agreement with that of the temperature fluctuation of the heated cylinder. For more detail explanation, however, the cir-

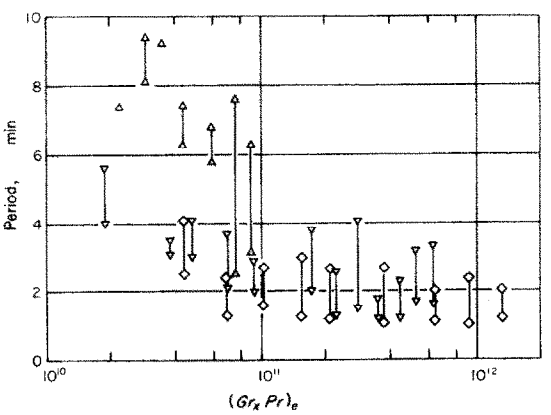

FIG. 28. Periods of the temperature fluctuation of the heated cylinder in water.

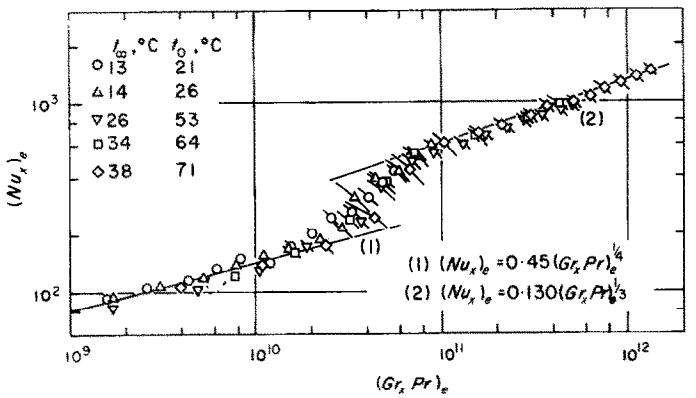

FIG. 29. Influence of the temperature fluctuations of the heated cylinder upon the values of $(Nu_x)_e$ and $(Gr_xPr)_e$ for water.

small relatively to the heat transfer rate, the wall temperature varies with the variation of the heat transfer rate to fluid, even when a constant rate of heat is supplied to the cylinder or plate from the rear side. In the schematic demonstration of Fig. 31, point M corresponds to Nu_x and Gr_xPr calculated from the time-mean values of the heat transfer rate and the wall temperature at a height x. Although the flow pattern at point P is turbulent, a laminar flow pattern is rather stable at that value of Gr_xPr. As soon as the flow changes to laminar, the heat transfer rate decreases and the wall temperature rises gradually. The above process may be indicated by the way of P → Q → R. At Gr_xPr corresponding to R the laminar flow pattern is unstable, therefore, it changes to turbulent. Then, the heat transfer rate increases and the wall temperature lowers gradually, that is, the process indicated by the way of R → S → P may be succeeded. The cycle of this process is repeated. The line P-M-R in Fig. 31 does not correctly correspond to any slanted bars in Fig. 29, since the variation with time of the heat transfer rate to fluid was not measured directly.

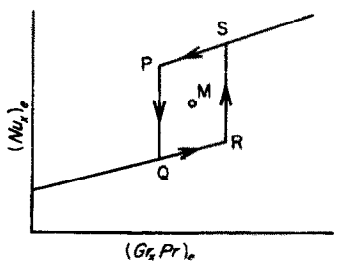

FIG. 31. Schematic explanation of the indeterminate character of the flow pattern of water.

Since the heat transfer coefficient to water is about five times larger than that to spindle oil under the same value of Gr_xPr, the remarkable temperature fluctuations of the heated cylinder perhaps appeared particularly in the former case. The same reason seems to be applicable to the explanation why special experimental equation (12) in turbulent region was evaluated exclusively for water. That is, the temperature fluctuation appears so as to even the heat transfer coefficient in the downstream of sufficiently large Gr_xPr, because of the effect of the indeterminate flow pattern in the transitional region as well as lack of the heat capacity of the heated cylinder. Therefore, under some relations between the heat capacity of the heated cylinder or plate and the heat transfer rate or between magnitudes of the length and the temperature difference in Gr_x, it can be presumed that the distinction between transition-turbulent and turbulent flow may possibly appear also in heat transfer to water, on the contrary, such a correlation as equation (12) may be possibly obtained also in heat transfer to other fluids.

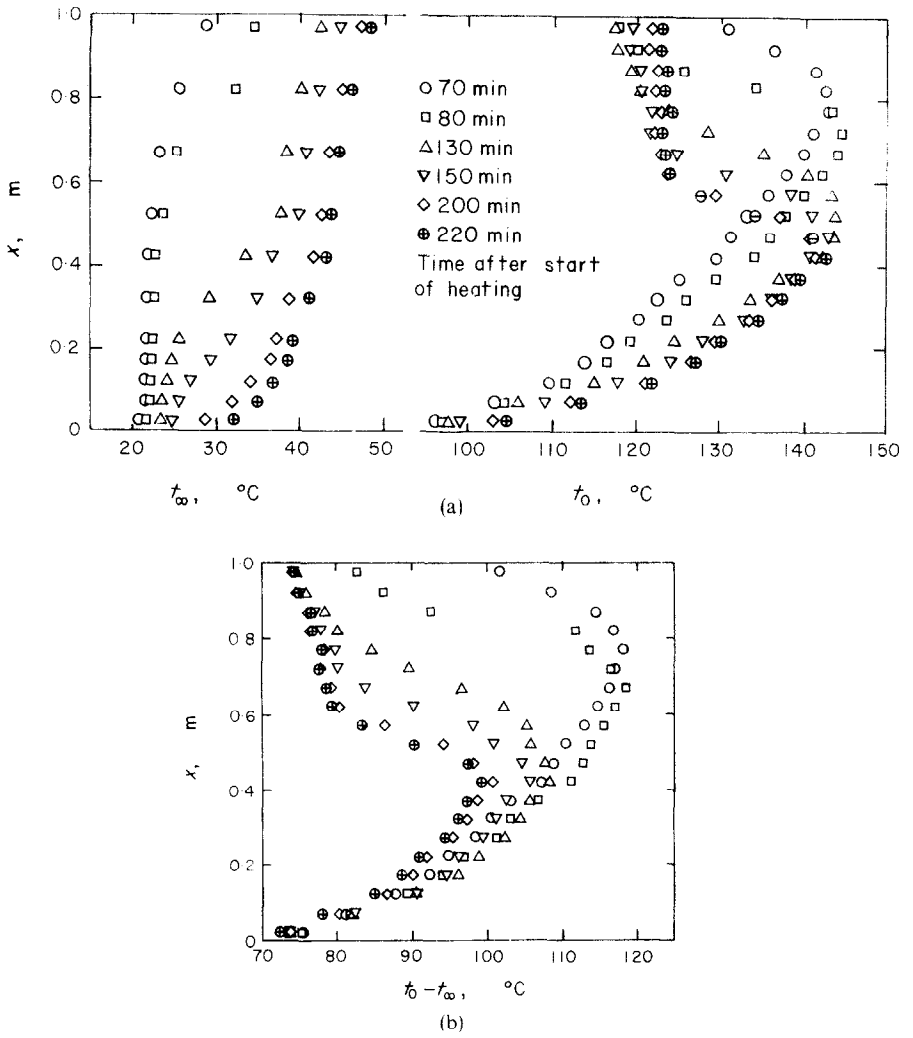

FIG. 32. Time-variation of the temperatures in quasi-steady state. (a) the heated cylinder and the ambient Mobiltherm oil. (b) temperature difference between the heated cylinder and the ambient Mobiltherm oil.

In the case of very small heat transfer rates as in air, an experimental equation similar to equation (12) may be obtained apparently, if such a experimental apparatus is used that the vertical conductive heat transfer inside the heated cylinder or plate tends to occur and if the heat transfer coefficient is calculated by using the heat rate supplied from the locally subdivided heat source. This case was realized in the experiments of Warner and Arpaci [22]. In their experiments, however, the temperature fluctuation of the heated plate must have been very small.

4.7 *Quasi-steady state and additional remarks on transition*

Figure 32(a) shows the time variation of the temperatures of the heated cylinder and the

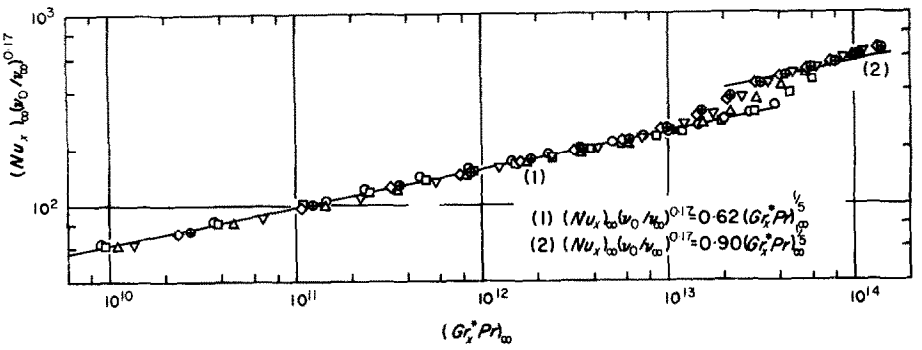

FIG. 33. Plot of $(Nu_x)_\infty\ (\nu_0/\nu_\infty)^{0.17}$ vs. $(Gr_x^*Pr)^\infty$ in the quasi-steady state for Mobiltherm oil.

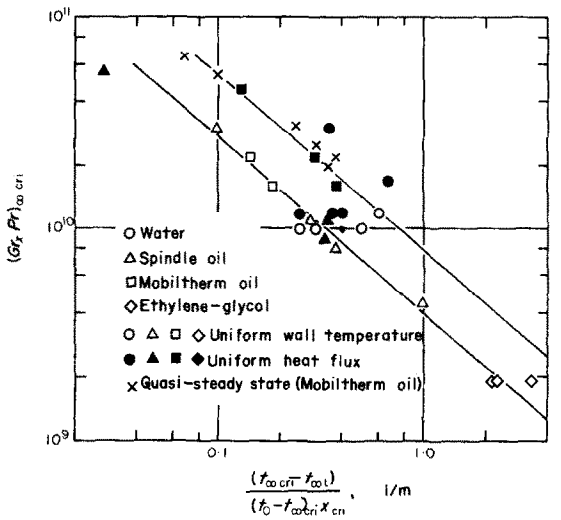

FIG. 34. Plot of $(Gr_xPr)_{\infty cri}$ upper limit of laminar region vs. $(t_{\infty cri}-t_{\infty l})/(t_0-t_\infty)_{cri}\,x_{cri}$ the grade of temperature stratification of the ambient fluid.

ambient fluid, when Mobiltherm oil was heated under the condition of uniform wall heat flux. As temperature stratification in the ambient is formed, the position of transitional region is gradually lowered, while the temperature distribution of the heated cylinder is remarkably affected. Steady state in its original sense was not attained even about three and a half hours after heating was started. After the distribution of the temperature differences between the heated cylinder and the ambient shown in Fig. 32(b) has approached a definite shape, both temperatures rise gradually to a certain level of steady state while maintaining this shape. This state was named as "quasi-steady state" [23].

Figure 33 shows the non-dimensional correlations of the heat transfer coefficients calculated from the data of Fig. 32. The data on laminar and

transition-turbulent region can be correlated by the same experimental equations as steady state respectively, though the transitional region varies. It may be therefore considered that the discord of the data on the portion of laminar region of Fig. 32(b) is due to the variation of physical properties with temperature. Hence the definition of quasi-steady state may be extended to a conception that it can be regarded to be the same as steady state with respect to the non-dimensional correlation of heat transfer coefficients. Its duration corresponds to the period from the end of transient convection to the beginning of steady state convection.

The experimental results for quasi-steady state suggest that the upper limits of laminar region $(Gr_xPr)_{cri}$ are affected by the vertical temperature gradients in the ambient. As this gradient becomes large, in fact it takes place that the temperature of the relatively outer part in the laminar boundary layer becomes lower than that of the ambient on the same level, namely, the buoyancy distribution which further promotes the development of vortex-pairs is formed.

A plot of $(Gr_xPr)_{\infty\,cri}$ vs. $(t_{\infty\,cri} - t_{\infty l})/(t_0 - t_\infty)_{cri}\,x_{cri}$ for all data presented in this paper is made as shown in Fig. 34, where x_{cri} is the height corresponding to the upper limit of laminar region, $(t_0 - t_\infty)_{cri}$ the temperature difference between the heated cylinder and the ambient on the level of x_{cri} and $(t_{\infty\,cri} - t_{\infty l})$ the difference between the ambient temperature on the level of x_{cri} and that of the lowest end of the heated cylinder. In the figure, are also plotted the data on ethylene-glycol from the experiments of [1] and on spindle oil from a supplemented experiment corresponding to $(t_{\infty\,cri} - t_{\infty l})/(t_0 - t_\infty)_{cri}\,x_{cri} = 1{\cdot}0$. From Fig. 34 it is found that

$$(Gr_xPr)_{\infty\,cri} = (4 \sim 8) \times 10^9 \times \left\{\frac{t_{x\,cri} - t_{\infty l}}{(t_0 - t_\infty)_{cri} \cdot x_{cri}}\right\}^{-0{\cdot}86},$$

and, at the same time, appreciated that the data on ethylene-glycol shown in Figs. 13(a) and 14 are not peculiar but reasonable. Apparently, the scattering of the data plotted in Fig. 34 may be ascribed mainly to the turbulence in the ambient and the data on quasi-steady state are appreciated to be affected by relatively small turbulence. The upper limit of laminar region corresponding to no temperature stratification and no turbulence in the ambient must be higher but uncertain.

The dependency of the transition from transition-turbulent to turbulent region on the experimental conditions was not found, since this transition was continuous.

5. CONCLUSION

Experimental studies on natural-convection heat transfer from a vertical cylinder to water, spindle oil and Mobiltherm oil were performed. The results of the experiments cover the range of $(Pr)_e = 2 \sim 300, (Gr_xPr)_e = 5 \times 10^7 \sim 5 \times 10^{12}$, $(Gr_x^*Pr)_e = 10^9 \sim 2 \times 10^{16}$ or $(Pr)_\infty = 4 \sim 2600$, $(Gr_xPr)_\infty = 9 \times 10^6 \sim 2 \times 10^{12}$, $(Gr_x^*Pr)_\infty = 4 \times 10^8 \sim 4 \times 10^{15}$. By subdividing the heater vertically into 20 sections, we could realize the conditions of uniform wall temperature and uniform heat flux, and measure local heat transfer coefficients.

From the observations on the boundary layer by means of the newly devised "mirage method" or other methods and from the measurements of the temperature field in the boundary layer by a thin thermocouple, we clarified the transition phenomena from the laminar to turbulent boundary layer as well as the characteristics of the turbulent boundary layer. Main conclusions are summarized as follows.

(1) The boundary layer develops through laminar, vortex-street, transition-turbulent and turbulent flow pattern, and each flow pattern has respective characteristics of heat transfer. Vortex-street flow pattern corresponds to transitional region on heat transfer. With respect to water, however, no distinction was found between transition-turbulent and turbulent flow.

(2) Two kinds of non-dimensional expressions

for heat transfer coefficients are proposed, respectively by using the physical properties at reference temperature t_e and by using the physical properties at ambient temperature t_∞ and the supplementary terms referred to the variation of kinematic viscosity. The experimental equations obtained by the latter, if the Nu number is multiplied by $(\nu_0/\nu_\infty)^{0.21}$ for the case of uniform wall temperature or $(\nu_0/\nu_\infty)^{0.17}$ for the case of uniform heat flux, agree with those obtained by the former, except for the turbulent region of spindle oil. The data on transitional region, however, are correlated better by the latter. Each Nu number is expressed by the function of the product $GrPr$ or Gr^*Pr in all regions within the accuracy of the experiments.

(3) The local and average heat transfer coefficients for the case of uniform wall temperature and the vertical temperature distributions of the heated cylinder for the case of uniform heat flux can be evaluated by Figs. 13(a), 14 and 13(b) or by their corresponding equations respectively. For the sake of approximate estimation of average heat transfer coefficients, equation (27) may be used in the range of $(Gr_L Pr)_\infty \geqslant 10^{10}$.

(4) With respect to the local heat transfer coefficients of transition-turbulent and turbulent region, each experimental equation for the case of uniform wall temperature and that of uniform heat flux can be transformed mutually by equation (19). Usually, the heated cylinder or plate is in some thermal conditions between uniform wall temperature and uniform heat flux. To these cases also, the equations for the case of uniform wall temperature may be applied generally except for laminar region.

(5) The transitional region corresponds with the process during which vortex-pairs are formed clearly and then collapsed. Consequently, the local heat transfer coefficients increase abruptly. When there are some factors to promote the development of vortex-pairs, Gr numbers corresponding to the transitional region become smaller. On the convection along a vertical cylinder, the grade of temperature stratification in the ambient is one of the most effective promoting factors as shown in Fig. 34. Owing to this uncertainty, the experimental equations recomended in this paper have some uncertain widths on their application range.

(6) The transition-turbulent region was primarily defined from the characteristics of heat transfer coefficients, and it is remarkable that equation (14) is applicable commonly to all fluids hitherto experimented. In this region, as the results of the collapse of vortex-pairs, the boundary layer thickness increases and the laminar sub-layer is formed. This region undergoes transition to turbulent region continuously.

(7) The turbulent boundary layer observed is not so homogeneous, as hitherto conceived, but violently disturbed lumps distribute irregularly in main boundary layer flow with less turbulence. The local heat transfer coefficients in this region increase with height at the rate of its one-fifth power. If the turbulence was homogenized when Gr number extensively increased, the characteristics of heat transfer coefficients would be altered. This prediction is reserved to be clarified by theoretical studies, since all theories hitherto proposed are inadequate.

(8) With respect to water, the temperature of the heated cylinder fluctuates with comparatively large periods and amplitudes. This phenomenon corresponds to the fact that the flow pattern of the boundary layer is indeterminate in the transitional region. Owing to that effect, the heat transfer coefficients in the turbulent region are vertically equalized. When the heat capacity of the heated wall is comparatively small to the heat transfer rates, such a phenomenon will possibly occur for other fluids too.

(9) Time-mean temperature profiles in the turbulent boundary layer can be correlated by non-dimensional temperature θ and a correlation variable ζ. The profiles are expressed in the same shape for both cases of transition-turbulent and turbulent flow, but in different shape for different kinds of fluid. The temperature fluctuations are considerably intense even at the part close to the heated cylinder, that is, at the part which is regarded as the laminar sub-layer.

(10) After the lapse of a certain period of transient convection, the heat transfer coefficients can be calculated by the experimental equations for steady state, but it should be noted that Gr number corresponding to the transitional region varies with the time-variation of the temperature stratification in the ambient. This unsteady state is defined as quasi-steady state.

ACKNOWLEDGEMENTS

The authors acknowledge the continued help and encouragement of Emeritus Prof. K. Yamagata and Prof. Nishikawa of Kyushu University. They are also grateful for a research scholarship from Matsunaga Science Foundation. Messrs. I. Morioka, H. Imura and M. Izumi assisted with the experiments and the manufacture of the apparatus, and Messrs. K. Ichiki, N. Nakamura, M. Shibata, H. Makino and T. Ishiodori took part in this investigation as their graduation thesis.

REFERENCES

1. T. FUJII, Experiments of free-convection heat-transfer from a vertical cylinder submerged in liquids, *Trans. Japan Soc. Mech. Engrs* **25**, 280–286 (1959).
2. T. FUJII, Experimental formula of free-convection heat-transfer from a vertical cylinder or a vertical plate, *Trans. Japan Soc. Mech. Engrs* **25**, 287–291 (1959).
3. T. FUJII, An analysis of turbulent free-convection heat-transfer from a vertical surface, *Trans. Japan Soc. Mech. Engrs* **25**, 292–298 (1959).
4. R. CHEESEWRIGHT, Turbulent natural convection from a vertical plane surface, *J. Heat Transfer* **90**, 1–8 (1968).
5. E. R. G. ECKERT and R. M. DRAKE, *Heat and Mass Transfer*, p. 324. McGraw-Hill, New York (1959).
6. E. R. G. ECKERT and T. W. JACKSON, Analysis of turbulent free-convection boundary layer on flat plate, *NACA TR* 1015, 255–261 (1951).
7. H. KATO, N. NISHIWAKI and M. HIRATA, On the turbulent heat transfer by free convection from a vertical plate, *Int. J. Heat Mass Transfer* **11**, 1117–1125 (1968).
8. E. R. G. ECKERT and E. SOEHNGEN, Interferometric studies on the stability and transition to turbulence of a free convection boundary layer, Proc. General Discussion on Heat Transfer, London, p. 321 (1951).
9. A. A. SZEWCZYK, Stability and transition of the free-convection layer along a vertical flat plate, *Int. J. Heat Mass Transfer* **5**, 903–914 (1962).
10. T. FUJII, An attempt of the analysis of the vortex streets developed in a free-convection boundary layer, *Trans. Japan Soc. Mech. Engrs* **25**, 276–280 (1959).
11. VDI, Wärmeatlas, Db 1, VDI-Verlag, Düsseldorf (1953).
12. S. OSTRACH, An analysis of laminar free-convection flow and heat transfer about a flat plate parallel to the direction of the generating body force, *NACA TR* 1111, 1–17 (1953).
13. T. FUJII, Heat-transfer from a vertical flat surface by laminar free-convection—The case where the physical constants of fluids depend on the temperature and the surface has an arbitrary temperature distribution in vertical direction, *Trans. Japan Soc. Mech. Engrs* **24**, 964–972 (1958).
14. S. AKAGI, Free convective heat transfer in viscous oil, *Trans. Japan Soc. Mech. Engrs* **30**, 624–635 (1967).
15. T. FUJII, H. UEHARA and N. FUJINO, Laminar free convection heat transfer from the outer surface of a vertical circular cylinder with uniform surface heat flux, Reports of Research Institute of Industrial Science, Kyushu University **43**, 1–12 (1966).
16. T. FUJII and H. UEHARA, Laminar natural convective heat transfer from the outer surface of a vertical circular cylinder, *Int. J. Heat Mass Transfer* (in press).
17. O. A. SOUNDERS, The effect of pressure upon natural convection in air, *Proc. R. Soc.* **A157**, 278–291 (1936).
18. O. A. SOUNDERS, Natural convection in Liquids, *Proc. R. Soc.* **A172**, 55–71 (1937).
19. K. YAMAGATA and M. KAWANO, Effective fluid temperature for heat transfer by laminar free convection, *Trans. Japan Soc. Mech. Engrs* **24**, 547–552 (1958).
20. Y. S. TOULOUKIAN, G. A. HAWKINS and M. JAKOB, Heat transfer by free convection from heated vertical surfaces to liquids, *Trans. Am. Soc. Mech. Engrs* **70**, 13–18 (1948).
21. T. FUJII, On the generation of a vortex street in the free-convection boundary layer, *Trans. Japan Soc. Mech. Engrs* **24**, 973–977 (1958).
22. C. Y. WARNER and V. S. ARPACI, An experimental investigation of turbulent natural convection in air at low pressure along a vertical heated flat plate, *Int. J. Heat Mass Transfer* **11**, 397–406 (1968).
23. K. YAMAGATA, T. FUJII and K. FUJINO, Free convection from a vertical plate to liquids in a relatively small vessel, *Kyudai Kogaku Shuho, Kyushu University* **27**, 35–40 (1954).
24. T. FUJII and I. MORIOKA, Measurements of thermal conductivities of liquids by a transient hot wire method, Reports of Research Institute of Industrial Science, Kyushu University **47**, 19–28 (1968).
25. T. FUJII and I. MORIOKA, Measurements of specific heat of liquids by a vacuum bottle, Reports of Research Institute of Industrial Science, Kyushu University **48**, 1–6 (1969).
26. N. E. DORSEY, *Properties of Ordinary Water-Substance*, p. 220. Reinhold, New York (1940).
27. P. L. GEIRINGER, *Handbook of Heat Transfer Media*, p. 164. Reinhold, New York (1962).

APPENDIX

Physical properties of water, spindle oil and Mobiltherm oil

The following formulas of physical properties were induced from the physical tables for water [11] and from the measured values for oils. The measurements of thermal

conductivity and specific heat are described in [24] and [25] respectively. Kinematic viscosity and density were measured with Ostwald's viscometers and standard scale areometers respectively.

For water;

$$\lambda = 0{\cdot}553 + 0{\cdot}255 \times 10^{-2}t - 0{\cdot}190 \times 10^{-4}t^2 + 0{\cdot}064 \times 10^{-6}t^3,$$

$$c = 4217 - 305 \times 10^{-2}t + 794 \times 10^{-4}t^2 - 825 \times 10^{-6}t^3 + 335 \times 10^{-8}t^4,$$

$$\nu \times 10^6 = 1{\cdot}792 - 6{\cdot}205 \times 10^{-2}t + 16{\cdot}009 \times 10^{-4}t^2 - 29{\cdot}780 \times 10^{-6}t^3 + 35{\cdot}314 \times 10^{-8}t^4 - 23{\cdot}075 \times 10^{-10}t^5 + 6{\cdot}240 \times 10^{-12}t^6,$$

$$\rho = 999{\cdot}9 + 2{\cdot}2 \times 10^{-2}t - 59{\cdot}5 \times 10^{-4}t^2 + 15{\cdot}9 \times 10^{-6}t^3.$$

In order to evaluate β, particularly, the following formula was induced from Dorsey's table [26].

$$\rho = 0{\cdot}9998905 + 0{\cdot}0061135 \times 10^{-2}t - 0{\cdot}0841538 \times 10^{-4}t^2 + 0{\cdot}0707211 \times 10^{-6}t^3 - 0{\cdot}0541866 \times 10^{-8}t^4 + 0{\cdot}0252936 \times 10^{-10}t^5 - 0{\cdot}0053173 \times 10^{-12}t^6.$$

The above formulas are approximated within the accuracy of 0·2, 0·004, 0·3, 0·01 and 0·001 per cent respectively.

For white spindle oil;

$$\lambda = 0{\cdot}1103 - 0{\cdot}0045 \times 10^{-2}t,$$

$$c = 1751 + 365 \times 10^{-2}t,$$

$$\log\log(\nu \times 10^6 + 0{\cdot}8) = -4{\cdot}03206 \log(t + 273{\cdot}15) + 10{\cdot}02259,$$

$$\rho = 887{\cdot}2 - 65{\cdot}5 \times 10^{-2}t.$$

The accuracy of the measurement in the above formulas is about 2, 1, 0·2 and 0·02 per cent respectively.

For Mobiltherm 600 oil;

$$\lambda = 0{\cdot}1123 - 0{\cdot}0025 \times 10^{-2}t,$$

$$c = 1663 + 336 \times 10^{-2}t,$$

$$\log\log(\nu \times 10^6 + 0{\cdot}8) = -4{\cdot}58263 \log(t + 273{\cdot}15) + 11{\cdot}67374,$$

$$\rho = 973{\cdot}3 - 0{\cdot}657t.$$

The accuracy of the measurement in the above formulas is the same order as spindle oil respectively. These values are deviated from Geiringer's data [27] to the order of 8, 8, 20 and 1 per cent respectively. It seems to be due to disparity of the materials.

EXPÉRIENCES SUR LE TRANSPORT DE CHALEUR PAR CONVECTION NATURELLE DANS DES LIQUIDES À PARTIR DE LA SURFACE EXTÉRIEURE D'UN CYLINDRE VERTICAL

Résumé—Cet article décrit les résultats de recherches expérimentales sur le transport de chaleur par convection naturelle à partir de la surface extérieure d'un cylindre vertical d'un mètre de haut dans de l'eau, de l'huile de machine et de l'huile Mobiltherm. Les caracteristiques des expériences sont comme suit. L'appareil expérimental est imaginé pour nous permettre de mesurer directement les coefficients de transport de chaleur local; des couches limites turbulentes suffisamment longues apparaissent sous diverses conditions de température et de flux de chaleur du cylindre chauffé; des correspondances entre les coefficients de transport de chaleur locaux et les configurations d'écoulement sont éclaircies à partir des observations de la couche limite au moyen de la "méthode du mirage" ou d'autres méthodes, et à partir des profils de température de la couche limite; l'influence du nombre de Prandtl sur le transport de chaleur est obtenue dans la gamme de 2 à 2600.

La couche limite croît en passant par des configurations d'écoulement laminaire, en rangée de tourbillons, de transition vers le turbulent et turbulent, et chaque configuration d'écoulement a des caractéristiques respectives de transport de chaleur. L'écoulement en rangée de tourbillons provoque une augmentation brusque des coefficients de transport de chaleur dans la région intermédiaire du laminaire à la transition vers le turbulent. Spécialement dans le cas de l'eau, aucune différence n'a été trouvée entre l'écoulement de transition vers le turbulent et le turbulent; ceci est expliqué par un caractère indéterminé de la configuration de l'écoulement dans la région intermédiaire. Les coefficients de transport de chaleur locaux sont corrélés de façon adimensionnelle pour chaque région d'écoulement dans les cas d'une température de paroi uniforme et d'un flux de chaleur uniforme. Dans chaque cas, deux sortes d'équations expérimentales sont proposées, respectivement, en employant les propriétés physiques à une température de référence et les termes supplémentaires relatifs à la variation de la viscosité cinématique. Les équations adimensionnelles des coefficients de transport de chaleur moyens sont proposés également dans le cas d'une température pariétale uniforme. De plus, quelques remarques sur les gammes appliquables à chaque équation sont présentées.

Les formes de paires de tourbillons, des sous-couches laminaires et des excroissances turbulentes dans la couche limite aussi bien que leurs développements, sont clairement vues dans les photos de "mirage".

Les transitions de la configuration de l'écoulement sont également décrites concrètement.

Les fluctuations de température dans la couche limite sont révélées et les profils de températures moyennées dans le temps sont représentés par un paramètre adimensionnel.

"L'état quasi-permanent" est défini expérimentalement comme un état équivalent à un état permanent par rapport aux coefficients de transport de chaleur.

VERGLEICHE ZUM WÄRMEÜBERGANG BEI FREIER KONVEKTION AN FLUIDE VON DEN AUSSENFLÄCHE EINES SENKRECHTEN ZYLINDERS

Zusammenfassung—Diese Arbeit beschreibt die Ergebnisse experimenteller Untersuchungen über den Wärmeübergang durch freie Konvektion an der Aussenfläche eines ein Meter hohen senkrechten Zylinders an Wasser, Spindelöl und Mobilthermöl. Bei den Versuchen wird auf folgende Besonderheiten geachtet: die Konstruktion der Versuchsapparatur ermöglicht die direkte Messung der örtlichen Wärmeübergangskoeffizienten; bei verschiedenen Temperaturen und Wärmestromdichten am beheizten Zylinder stellen sich stets genügend lange turbulente Grenzschichten ein; durch Beobachtung der Grenzschicht mit Hilfe der "Schatten-Methode" oder anderer Verfahren und durch Messung der Temperaturprofile können die Zusammenhänge zwischen den örtlichen Wärmeübergangskoeffizienten und dem Strömungszustand ermittlelt werden; es soll der Einfluss der Prandtlzahl auf den Wärmeübergang im Bereich $Pr = 2$–2600 gefunden werden.

Die Grenzschicht durchläuft Stadien mit laminarer Strömung, Strömung mit Wirbelstrassen, ein Übergangsgebiet zu turbulenter Strömung und erreicht schliesslich vollturbulente Strömung. Jeder Strömungszustand zeigt besondere Wärmeübergangsverhältnisse. Wirbelstrassenströmung bewirkt ein plötzliches Ansteigen des Wärmeübergangs im Übergangsgebiet von laminarer zu turbulenter Strömung. Bei Wasser insbesondere konnte nicht unterschieden werden zwischen Übergangsbereich und vollturbulenter Strömung. Als Grund wird die Unbestimmtheit des Strömungsstandes im Übergangsgebeit angegeben.

Zu jedem Strömungszustand werden dimensionslose Gleichungen für die örtlichen Wärmeübergangskoeffizienten aufgestellt, sowohl für den Fall konstanter Wandtemperatur als auch konstanter Wärmestromdichte. Für jeden der beiden Fälle werden zwei experimentell gefundene Gleichungen vorgeschlagen, wobei einmal die physikalischen Eigenschaften bei einer Bezugstemperatur und zum anderen Hilfswerte, die die Änderung der kinematischen Zähigkeit berücksichtigen, verwendet werden. Ausserdem werden dimensionslose Gleichungen für den mittleren Wärmeübergangskoeffizienten bei konstanter Wandtemperatur vorgeschlagen. Es werden einige Bemerkungen zum Anwendungsbereich jeder Gleichung gemacht.

Das Aussehen von Wirbelpaaren, laminaren Unterschichten und Turbulenzballen in der Grenzschicht ebenso wie ihre Entwicklung sind in "Schatten-Aufnahmen exakt festgehalten. Auch die Übergänge zwischen zwei Strömungszuständen sind genau beschrieben.

Es werden Temperaturschwankungen in der Grenzschicht nachgewiesen. Die zeitlich gemittelten Temperaturprofile werden durch einen dimensionslosen Parameter dargestellt. Der quasi-stationäre Zustand" wird aus den Versuchen definiert als ein Zustand, der im Hinblick auf die Wärmeübergangskoeffizienten gleichbedeutend mit dem stationären Zustand ist.

ЭКСПЕРИМЕНТЫ ПО ТЕПЛООБМЕНУ ОТ ВНЕШНЕЙ ПОВЕРХНОСТИ ВЕРТИКАЛЬНОГО ЦИЛИНДРА К ЖИДКОСТЯМ В УСЛОВИЯХ ЕСТЕСТВЕННОЙ КОНВЕКЦИИ

Аннотация—В статье описываются экспериментальные результаты по теплообмену от внешней поверхности вертикального цилиндра высотой 1 м к воде и различным типам смазочных масел. Экспериментальная установка позволила непосредственно измерять локальные коэффициенты теплообмена. Достаточно длинные турбулентные слои возникают при различных температурах и тепловых потоках нагреваемого цилиндра. Связь между локальными коэффициентами теплообмена и характеристиками потока получены в результате наблюдений различными методами за пограничным слоем, а также благодаря изменениям температурных профилей в потоке; обнаружено влияние числа Прандтля на теплообмен в диапазоне изменения Pr от 2 до 2600.

Пограничный слой образуется при ламинарном, вихревом, переходном и турбулентном потоках, причем каждый вид движения имеет соответствующие ему характеристики

теплообмена. Вихревое движение вызывает внезапное увеличение интенсивности теплообмена в переходной области между ламинарным и турбулентным и режимами. Для воды не обнаружено различий между турбулентным и переходным течениями, его возникновение обнаруживается неопределенным характером течения в переходной зоне.

Локальные коэффициенты теплообмена представлены в безразмерном виде почти для каждого режима течения для 2-х случаев: постоянной температуры стенки и постоянного теплового потока. Для каждого случая, соответственно, предлагаются два вида эмпирических формул; физические свойства выбираются по начальной температуре; дополнительные члены учитывают изменение кинематической вязкости. Также предлагаются безразмерные уравнения для расчета средних коэффициентов теплообмена, когда температура стенки постоянна. Кроме того, сделаны указания по области применимости каждого уравнения. Показаны на фотографиях формы парных вихрей, ламинарные подслои и турбулентные кромки пограничного слоя и их развитие. Также описываются переходные режимы течения.

Обнаружены отклонения температуры в пограничном слое, а профили температуры, осредненные во времени представлены в зависимости от безразмерного иараметра.

Экспериментально выявлено квазистационарное состояние, соответствующее стационарному состоянию по отношению к коэффициентам теплообмена.